Journal of Medicinal Chemistry

Article

Synthesis and in vivo Biological Evaluation of 68Ga Labelled Carbonic Anhydrase IX Targeting Small Molecules for Positron Emission Tomography

Deborah Sneddon, Raymon Niemans, Matthias Bauwens, Ala Yaromina, Simon J.A. van Kuijk, Natasja Gabi Lieuwes, Rianne Biemans, Ivo Pooters, Paul A. Pellegrini, Nigel A Lengkeek, Ivan Greguric, Kathryn F. Tonissen, Claudiu T Supuran, Philippe Lambin, Ludwig Dubois, and Sally-Ann Poulsen

J. Med. Chem., **Just Accepted Manuscript** • DOI: 10.1021/acs.jmedchem.6b00623 • Publication Date (Web): 20 Jun 2016

ACS Publications

Journal of Medicinal Chemistry is published by the American Chemical Society. 1155 Sixteenth Street N.W., Washington, DC 20036

Abstract

Tumor hypoxia contributes resistance to chemo- and radiotherapy, while oxygenated tumors are sensitive to these treatments. The indirect detection of hypoxic tumors is possible by targeting carbonic anhydrase IX (CA IX), an enzyme overexpressed in hypoxic tumors, with sulfonamide-based imaging agents. In this study, we present the design and synthesis of novel gallium radiolabelled small molecule sulfonamides targeting CA IX. The compounds display favorable in vivo pharmacokinetics (PK) and stability. We demonstrate that our lead compound, [^{68}Ga]-**2**, discriminates CA IX expressing tumors in vivo in a mouse xenograft model using positron emission tomography (PET). This compound shows specific tumor accumulation, low uptake in blood and clears intact to the urine. These findings were reproduced in a second study using PET/CT (computed tomography). Small molecules so far investigated utilizing ^{68}Ga for preclinical CA IX imaging are scarce and this is one of the first effective ^{68}Ga compounds reported for PET imaging of CA IX.

Introduction

Molecular imaging with positron emission tomography (PET) has had a profound impact on primary diagnosis, management, therapy monitoring and prognosis in cancer; it is noninvasive and provides personalized care to patients by informing treatment decisions and evaluating treatment response. Hypoxia (low oxygen concentration) is a characteristic feature of solid tumors. Hypoxic cells co-opt adaptive mechanisms to switch to a glycolytic metabolism, promote cell proliferation, evade immune attack, induce angiogenesis, invade and metastasize.[1] Tumor hypoxia is a negative prognostic factor associated with a more aggressive phenotype, specifically with resistance to chemo- and radiotherapy. For example, up to a 3-fold higher radiation dose is needed to achieve the same level of tumor cell death in hypoxic tumors compared to oxygenated tumors.[2] The implementation of a hypoxia-guided clinical management strategy, such as hypoxia radiation sensitizers (e.g. nimorazole[3]) or hypoxia specific cytotoxic therapy e.g. TH-302 (Figure 1A)[4] to those patients most likely to benefit is currently not possible as there is no established method in routine clinical practice that is: (i) non invasive, (ii) routine to prepare, and (iii) indicative of the hypoxic cell population [2] Most current methods to detect hypoxia are invasive (e.g. require surgery) and are subject to technical issues causing sampling errors.

Small molecule molecular probes for imaging of hypoxia with PET may be split into two broad categories, 'direct' or 'indirect' imaging probes. Nitroimidazoles are direct imaging probes for the detection of hypoxia with PET, with one compound, ^{18}F-fluoromisonidazole (^{18}F-FMISO) in limited clinical use.[5] Second and third generation nitroimidazoles, ^{18}F-FAZA and ^{18}F-HX4, respectively, have been shown by us to address the PK problems of ^{18}F-FMISO (slow tumor-specific accumulation and nonspecific washout), however, better probes for hypoxia are still required.[5-8]

A critical cellular response to hypoxia is the stabilisation and activation of the transcription factor hypoxia inducible factor-1α (HIF1α). HIF1α regulates the expression of genes required for survival under hypoxia. In principle, the gene products may be used as targets for imaging of tumor hypoxia with indirect probes and bypass the drawbacks associated with nitroimidazole probes.[9] Carbonic anhydrase IX (CA IX) is one of the most highly induced HIF1α responsive genes and is proposed as the "gold standard" endogenous marker of cellular hypoxia.[10-13] CA IX expression is a negative prognostic factor in several types of cancer.[14] Additionally CA IX (over)expression is thought to predict the therapeutic effect of CA IX-targeting anticancer therapies. CA IX is overexpressed and sustained in many solid tumors including breast, brain (glioblastoma), clear cell renal, colorectal, head and neck, bladder and non-small cell lung carcinomas but expression in normal tissues is restricted to the stomach and GI tract.[10, 15]

CA IX is a transmembrane zinc metalloenzyme that catalyzes the reversible hydration of CO_2 to HCO_3^- and H^+, enabling the tumor to regulate pH allowing its spread and survival.[12, 13, 16-20] Expression of CA IX is commonly used as a histologic marker of tissue hypoxia, with detection using M75[18] or G250[21], two different monoclonal antibodies specific for CA IX. There are several antibody and antibody fragment based imaging agents with in vivo data that indirectly target hypoxic tumors by binding to CA IX.[22, 23]

Our groups have shown that small molecule sulfonamides are able to discriminate oxygen levels in tissues and bind preferentially to CA IX only in hypoxic cells, while CA IX targeting antibodies also bind upon reoxygenation.[24] Therefore our attention has turned to small molecules to develop radiopharmaceuticals to detect CA IX positive tumors with PET. Very few indirect small molecules that that incorporate a primary sulfonamide functional group,

required for tight binding to the active site zinc CA IX (see examples in Figure 1) have so far been developed and tested for CA IX imaging with PET in vivo.[25-29] Compound [^{18}F]U-104 proved ineffective due to poor PK.[28] [^{18}F]VM4-037 was found to be safe for use in healthy volunteers[25], but no CA IX dependent uptake was found in vivo.[30, 31] In a recent phase II pilot study of two patients with clear cell renal cell carcinoma (RCC) primary tumors with this agent uptake was observed in both healthy and cancerous kidney as well as metastases, and CA IX selectivity was not confirmed[32], limiting the use of this imaging agent in RCC. Only the trivalent sulfonamide compound, [^{18}F]AmBF$_3$-(ABS)$_3$, to date demonstrates imaging efficacy in vivo.[26] [^{18}F]AmBF$_3$-(ABS)$_3$, enabled tumor visualisation with a tumor to blood ratio (TBR) of 2.88 ± 1.81 in CA IX-expressing HT-29 tumors 1 h after injection, interestingly its monovalent variant, AmBF$_3$-ABS, was ineffective.[26] No discrimination was shown between CA IX-expressing or non-expressing tumors, however, pre-injection of acetazolamide effectively blocked uptake of [^{18}F]AmBF$_3$-(ABS)$_3$ in the tumor. Recently another series of mono-, di- and trivalent sulfonamides based on ^{68}Ga-DOTA as the PET reporter group were tested in a CA IX-expressing HT-29 tumor xenograft, again only the trivalent sulfonamide had a TBR that significantly differed to that of controls (where test animals are first treated with acetazolamide as a CA IX blocking sulfonamide).[27]

^{68}Ga ($t_{1/2}$ = 68 minutes) has been used to label small molecules, biological macromolecules as well as nano- and micro-particles.[33] It is a favourable positron emitter because its γ emission is negligible and it can be produced in a ^{68}Ge/^{68}Ga generator, an on-site cyclotron is not required.[34] As the parent radionuclide ^{68}Ge has a long half life ($t_{1/2}$ = 270.8 days) it can be stored for relatively long periods.[34] To make PET imaging with sulfonamides suitable for eventual use in cancer patients, the purpose of the present work is to design and synthesize novel small molecule ^{68}Ga labelled imaging agents that can selectively target CA IX positive

tumor cells in vivo. Specifically, agents with improved PK properties, CA IX targeting, TBR and image contrast than those previously described are sought.

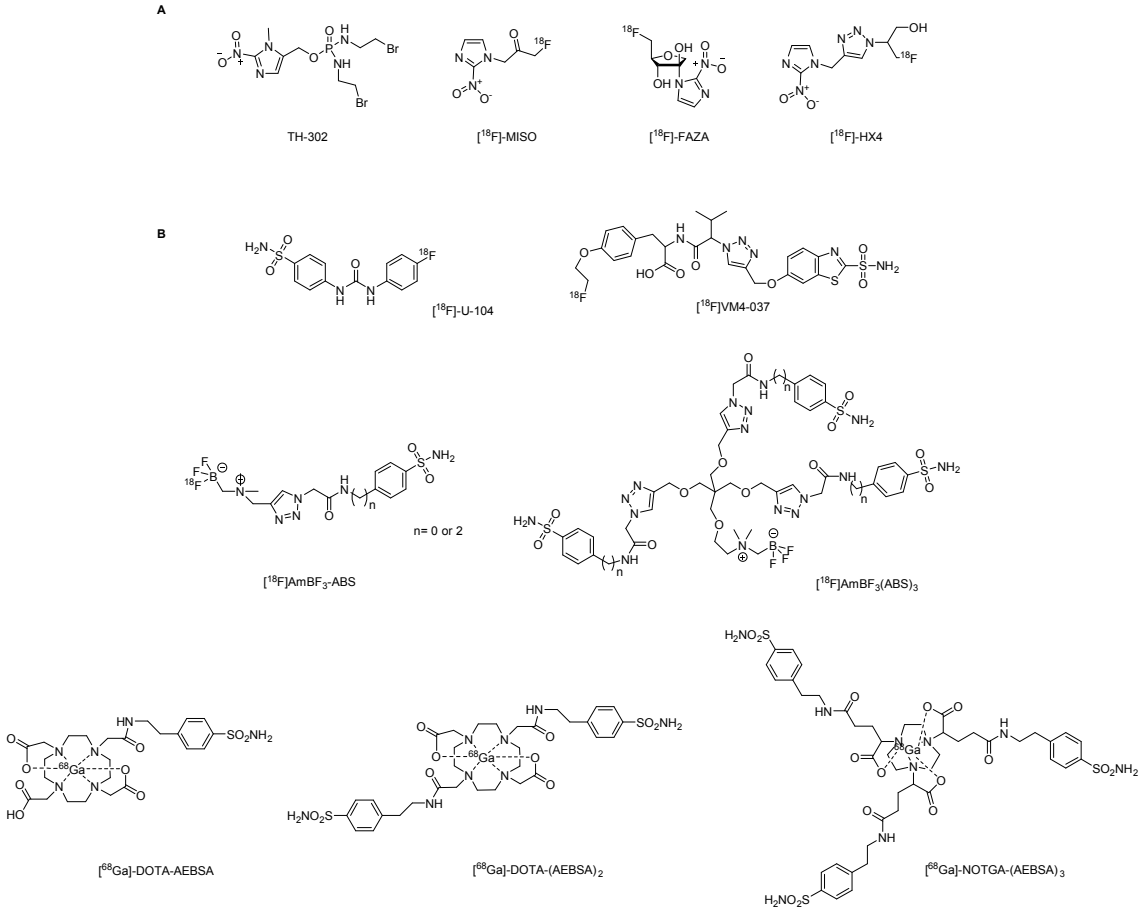

Figure 1: A) Nitroimidazole hypoxia targeted cytotoxic drug TH-302 and small molecule nitroimidazole PET imaging agents for hypoxia: ^{18}F-MISO, ^{18}F-FAZA and ^{18}F-HX4. B) Small molecule primary sulfonamides investigated in animal models for CA IX imaging with PET.[25-28]

Results and discussion

Compound design and synthesis. Most small molecule CA inhibitors incorporate a primary sulfonamide functional group, which imparts molecular recognition specificity for the zinc in

the active site of CAs, but not the metal of other metalloenzymes.[29] The active site of CA IX is, however, structurally similar to CA I and CA II, the major CA isozymes within red blood cells, (CA I: 1.6 ± 2.3 mg/g hemoglobin (Hb); CA II: 1.8 ± 0.3 mg/g Hb).[35] As a consequence of the binding of sulfonamide based imaging agents to CA I and II in red blood cells, increased background signal and reduced image contrast have hampered the efforts of others in this field.[2, 36, 37] Our group has contributed substantially to the development of CA inhibitors with enhanced selectivity for CA IX over CA I and CA II in vitro, and via extrapolation, in vivo.[4] We have shown that the different CA active sites have variable tolerance to the nature of moieties appended to the aromatic sulfonamide CA targeting group.[38-42] This attribute allows fine-tuning of the bioactivity, physicochemical and toxicological properties of the compound to better target a particular CA isozyme.[43] The CA IX targeting agents of this study, compounds **1** (^{nat}Ga and ^{67}Ga) and **2** (^{nat}Ga, ^{67}Ga and ^{68}Ga) extend on our established design principles. These compounds are primary sulfonamides tethered to a metal chelator, DOTA (1,4,7,10-tetraazacyclododecane-1,4,7,10-tetraacetic acid) via either an intervening aliphatic triazole linker (**1**) or hydrophilic triazole PEG linker (**2**), Figure 2. The DOTA macrocycle is the workhorse metal ion chelator for molecular imaging agents, forming stable complexes with the PET imaging isotope Gallium-68, ^{68}Ga.[44] ^{68}Ga is becoming a relevant isotope for routine clinical examinations with ^{68}Ga PET imaging agents such as ^{68}Ga-DOTATATE and ^{68}GaHBED-PSMA in clinical use.[45, 46] ^{67}Ga is a common radionuclide for use with Single Photon Emission Computed Tomography (SPECT). The most widely used application is of ^{67}Ga-citrate for inflammation and infection imaging. The relatively long half-life ($t_{1/2}$ = 3.26 days) makes ^{67}Ga a useful tool for the assessment of key parameters of gallium-based radiopharmaceuticals; including radiochemical stability, metabolic stability and plasma protein binding, this in turn informs subsequent decisions on in vivo protocols. The preparation of ^{67}Ga complexes also permits the optimization of

radiolabelling conditions, purification methodology and reformulation procedures prior to using the shorter half-life PET radionuclide ^{68}Ga. We first synthesised the 'cold' compounds, ^{nat}Ga-**1** and ^{nat}Ga-**2**, followed by the corresponding radiolabelled compounds ^{67}Ga-**1** and ^{67}Ga-**2** to establish optimized radiolabelling conditions. ^{68}Ga-**2** was selected as the target compound for in vivo PET imaging studies.

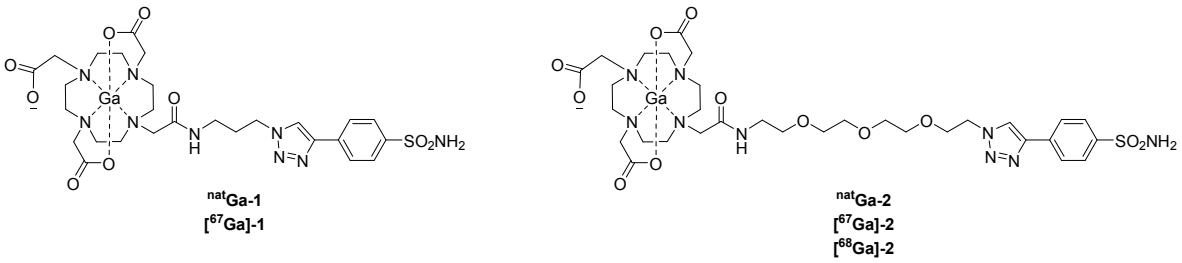

Figure 2: Target [sulfonamide]-[triazole linker]-[DOTA] compounds for use as CA IX imaging agents.

The compound design as [sulfonamide]-[variable linker]-[DOTA] is deliberately modular. This enables a straightforward synthesis using copper catalyzed azide-alkyne cycloaddition (CuAAC), or 'click chemistry', to combine the components. CuAAC is one of the most accomplished reactions for combining groups to pool their individual properties into a single molecule.[47] The biopharmaceutical stability of the resulting triazole is favourable, it is resistant to acidic, basic, reductive, oxidative conditions in addition to enzymatic degradation.[48] Scaffold **2** employs a tetraethylene glycol linker, which is a shortened polyethylene glycol (PEG) chain with good biopharmaceutical properties, polarity and water solubility, aiding the eventual formulation.[49] The PEG-based linker was additionally selected to enhance the likelihood that the agents would have improved specificity for CA IX. The increased polarity reduces plasma protein binding and membrane permeability and thus may lessen the off-target binding to CA I and II in red blood cells.[50] A previous generation of

DOTA based scaffolds were designed by Rami et al but to the best of our knowledge, these were not radiolabelled or evaluated as CA IX imaging agents in vivo.[51, 52]

Target compounds **1** and **2** are synthesized from three modular components, [sulfonamide], [linker] and [DOTA], with incorporation of the gallium cation as the final step (Scheme 1 and 2). The synthesis of the [sulfonamide] component, 4-ethynyl benzene sulfonamide **5**, has been described previously.[53] The [linker] components, **4** and **11**, were designed with orthogonal end groups. An azide facilitates reaction with **5** via CuAAC, while the bromide provides an orthogonal leaving group facilitating the S_N2 substitution reaction with the [DOTA] component **7**. Linkers **4** and **11** were prepared by reaction of bromoacetylbromide (3.3 equiv) with the amino azides **3**[54] and **10,** respectively.[55] The [sulfonamide] **5** and [linker] components **4** and **11** were subjected to $CuSO_4$ (0.01 equiv), sodium ascorbate (0.1 equiv) and TBTA (0.01 equiv) to generate **6** and **12**, respectively. The removal of excess copper ions from **6** and **12** was achieved by a solid EDTA chase or by washing the organic phases with EDTA (1.0 M) in ammonium hydroxide (28.0-30.0%, NH_3 basis) solution. The [DOTA] component **7** was prepared from commercially available cyclen as described by Prashun et al.[56] S_N2 substitution of **6** and **12** with **7** using anhydrous conditions gave the *t*Bu-protected compounds **8** and **13** in reasonable yields. Treatment of compounds **8** and **13** with either neat formic acid or TFA/DCM (1:1) removed the *t*Bu protecting groups to provide the non-metallated precursor compounds **9** and **14** in high yield. Next, the target ^{nat}Ga complexes, ^{nat}Ga-**1** and ^{nat}Ga-**2**, were prepared in quantitative yield from **9** and **14** using $Ga(NO_3)_3 \bullet xH_2O$ in H_2O with pH adjusted to pH 4.5 with 1.0 M HCl or 1.0 M KOH. Compounds **9** and **14** were purified by reverse-phase HPLC prior to biological evaluation and radiolabelling with ^{67}Ga and/or ^{68}Ga.

Scheme 1. Synthesis of [^{nat}Ga]-**1**.[a]

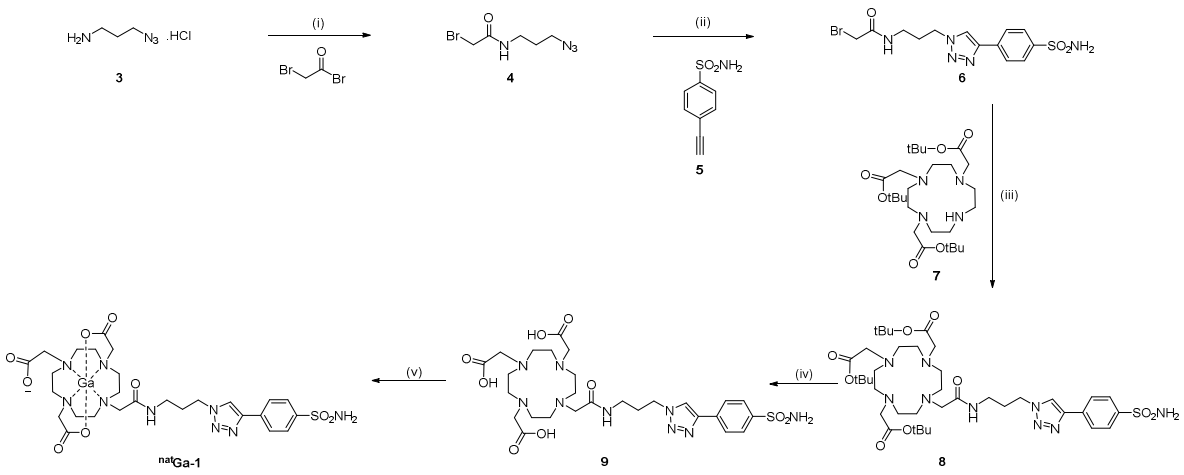

[a]Reagents and conditions: (i) Bromoacetylbromide (3.3 equiv), 1.0 M aqueous NaOH (3 equiv), DCM, rt, 18 h ; (ii) Compound **5** (1.0 equiv), $CuSO_4$ (0.05 equiv), sodium ascorbate (0.1 equiv), TBTA (0.05 equiv), 2:1 DMSO:H_2O, 45 °C, 3 h (iii) Compound **7** (1.2 equiv), K_2CO_3 (1.2 equiv), anhyd MeCN, rt, 18 h; (iv) 1:1 TFA:DCM, rt, 18 h (v) $Ga(NO_3)_3 \bullet xH_2O$ (1.1 equiv), H_2O, 80 °C, 2-4 h.

Scheme 2. Synthesis of [^{nat}Ga]-**2**.[a]

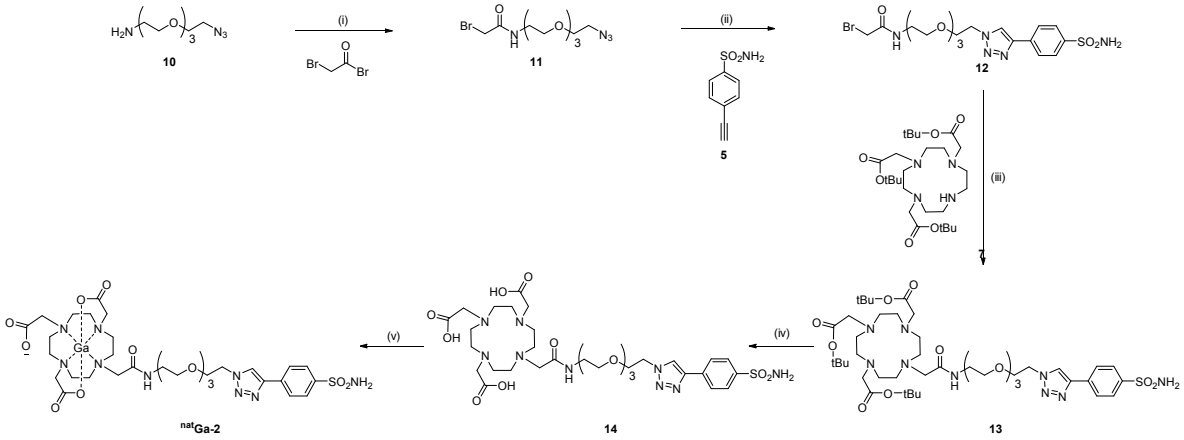

[a]Reagents and conditions: (i) Bromoacetylbromide (3.3 equiv), NaOH (1.0 M, 2 equiv), DCM, rt, 18 h ; (ii) Compound **5** (1.0 equiv), $CuSO_4$ (0.01 equiv), sodium ascorbate (0.1

equiv), TBTA (0.01 equiv), 2:1 DMSO:H_2O, 30 °C, 18 h (iii) Compound **7** (1.2 equiv), K_2CO_3 (1.3 equiv), anh MeCN, 60 °C, 3 h; (iv) 1:1 TFA:DCM, rt, 18 h (v) $Ga(NO_3)_3 \bullet xH_2O$ (1.1 equiv), H_2O, 80 °C, 2-4 h.

Carbonic Anhydrase Binding

The CA binding data for ^{nat}Ga-**1**, ^{nat}Ga-**2** and the reference CA inhibitor acetazolamide were measured for the cancer-associated CA isozymes, CA IX and XII, and off target CA isozymes, CA I and II. Compounds ^{nat}Ga-**1** and ^{nat}Ga-**2** have low affinity for CA I, but bind equally well to CA II, CA IX and CA XII (K_i range 59.6 – 84.7 nM) (Table 1). Binding to CA II supports the significance and importance of designing probes to have reduced cell membrane permeability as this limits access of the probes to the intracellular CA II.

Table 1. Inhibition data for human CA isozymes I, II, IX and XII with compounds ^{nat}Ga-**1**, ^{nat}Ga-**2** and reference compound acetazolamide.

	***K*$_i$ (nM)**[a,b]				**Selectivity**[c]		
Compd	hCA I	hCA II	hCA IX	hCA XII	CA I/CA IX	CA II/CA IX	CA XII/ CA IX
acetazolamide[d]	250	12	25	n/a	10	0.48	n/a
^{nat}Ga-**1**	387	72.5	84.7	59.6	4.57	0.85	0.70
^{nat}Ga-**2**	169	78.3	63.1	56.8	2.67	1.24	0.90

[a]Errors in the range of ± 5% of the reported value, from three determinations. [b]Measured using a stopped flow assay that monitors the physiological reaction (CA catalysed hydration of CO_2).[57, 58]

[c]Selectivity is determined by the ratio of K_is for CA isozymes I, II and XII relative to CA IX.[d] Literature AZA values[59]

Radiochemistry

Compounds **9** and **14** were successfully radiolabelled with ^{67}Ga under standard conditions, 0.1 M sodium acetate, pH 4.5, 10 min, 95 °C. To test the robustness of the radiolabelling method developed, the compound amount was reduced from 10 nmol progressively to 1 nmol and the radiochemical yield quantified by reverse-phase HPLC (Table 2). It was shown that **9** → [^{67}Ga]-**1** was successfully radiolabelled down to 2 nmol of compound (98%) but at 1 nmol, only 61% radiolabelling was achieved. However, **14** → [^{67}Ga]-**2** radiolabelled efficiently down to 1 nmol compound (>99%). Purification of radiolabelled products was carried out using either RP-HPLC or rapid reverse phase C-18 solid phase extraction (SPE). Both [^{67}Ga]-**1** and [^{67}Ga]-**2** were reformulated into PBS.

Table 2. Radiochemical yield of [^{67}Ga]-**1** and [^{67}Ga]-**2** at varying compound concentrations.[a]

Compound amount	**Radiochemical yield (%)**[b]	
(nmol)	**9 →**[^{67}Ga]-**1**	**14 →** [^{67}Ga]-**2**
25	100[c]	100
10	98 ± 1.4[d]	98.5 ± 0.7[d]
5	n/a	>99

2	98	100
1	61	>99

[a]Reaction conditions: Compound **9** or **14** (1 mM in water), sodium acetate (0.1 M, to pH 4.5), $^{67}GaCl_3$ (18-21 MBq in 0.1 M HCl), 95 °C, 10 min. [b]As determined by RP-HPLC (conditions available in supporting information). [c]Labelling in HEPES buffer proceeded with >99% radiochemical yield. [d]± standard deviation based on two radiolabelling experiments.

Compound **14** was radiolabelled with ^{68}Ga (200-800 MBq), eluted from a $^{68}Ge/^{68}Ga$ generator (IDB Holland, The Netherlands) in about 1 mL, in 400 µL in 3.0 M sodium acetate or ammonium acetate, pH 4.3, 10 min, 99 °C in high radiochemical purity (> 95%,) as determined by radio-RP-HPLC (Inertsil ODS C18, 5 µM, 4.6 × 250 mm, 100:0 → 0:100 H_2O + 0.1% TFA/MeCN + 0.1% TFA, 1.0 mL/min).

Biopharmaceutical properties

The stability of ^{67}Ga radiolabelled compounds [^{67}Ga]-**1** and [^{67}Ga]-**2** was examined in phosphate buffered saline (PBS), pH 7.4. The compounds were found to be stable, with ≥95% of the parent compounds remaining after 18 h incubation at 37.5 °C and ≥90% after 96 h incubation. The protein binding of [^{67}Ga]-**1** and [^{67}Ga]-**2** to human serum was minimal (< 7%, n = 3) after 48 h. [^{67}Ga]-**2** exhibited favourable radiochemical purity (data not shown), good stability and good preliminary physicochemical properties, hence additional biopharmaceutical properties of cold ^{nat}Ga-**2** were assessed (Table 3), by extrapolation these properties should reflect those expected for the radiolabelled analogue [^{68}Ga]-**2**. The in vitro metabolic stability of compound ^{nat}Ga-**2** in mouse liver microsomes was measured in the presence and absence of NADPH, the cofactor required for oxidative metabolism by

CYP450s. Compound ^{nat}Ga-**2** exhibited minimal microsomal degradation ($t_{1/2}$ > 247 min) and it is expected that compound ^{nat}Ga-**2** is subject to low hepatic clearance in vivo. The *in vitro* intrinsic clearance of ^{nat}Ga-**2** was low (< 7 µL/min/mg protein). The in vitro membrane permeability (Papp) of ^{nat}Ga-**2** in the Caco-2 cell model (pH 7.4) was measured. ^{nat}Ga-**2** was not detected in the Caco-2 assay acceptor chamber, while good mass balance (92% ± 6%) confirmed minimal retention of the compound within the cell monolayer and minimal nonspecific adsorption. The experimental value measured, Papp <0.7 cm s^{-1}, indicates that ^{nat}Ga-**2** has very low cell membrane permeability. The stability and extent of plasma protein binding of ^{nat}Ga-**2** in mouse plasma was analyzed. The measured concentration of ^{nat}Ga-**2** in mouse plasma samples (37 °C) quenched at 2 min was unchanged. However, at 10 min, the concentration of ^{nat}Ga-**2** had dropped but then remained steady over the remainder of the 4 h incubation. Plasma protein binding of ^{nat}Ga-**2** was low (39%) following 4 h incubation. Cytotoxicity and cell viability of ^{nat}Ga-**2** were tested via a standard methyl thiazolyl tetrazolium assay, with no toxicity observed up to 1 mM of ^{nat}Ga-**2** in normoxia (data not shown). Collectively, these additional properties of ^{nat}Ga-**2** are indicative of a safe, well tolerated compound with physicochemical properties suited to preferential targeting of CA IX over intracellular CAs; hence a favorable TBR ratio of the corresponding ^{68}Ga compound.

Table 3. Biopharmaceutical properties of compound ^{nat}Ga-**2**

Compd	**Degradation $t_{1/2}$ (min)**[a]	***In vitro* CLint (µL/min/mg protein)**[a]	**Microsome-Predicted E_H**[b]	**Papp ($cm.s^{-1}$)**[c]	**Plasma protein binding (4 h)**[d]
^{nat}Ga-**2**	>247	<7	<0.13	<0.7	39%

[a]Values are represented as mean ± SD (n = 3). Metabolic stability parameters for compound ^{nat}Ga-**2** based on NADPH-dependent degradation profiles in mouse liver microsomes. In vitro

intrinsic clearance value (CLint, in vitro). [b]Predicted in vivo hepatic extraction ratio (E_H). [c] Papp = apparent permeability across Caco-2 monolayers. [d]Values are the average of duplicate determinations.

Small animal imaging PET and PET/CT studies

Our lead compound, [^{68}Ga]-**2**, was chosen for follow up in vivo PET studies and has been injected intravenously in mice bearing HCT116 tumors with high or low CA IX expression to assess selectivity of uptake using PET. The efficiency of CA IX genetic silencing was determined by Western blot analysis and immunofluorescence. In agreement with previous studies,[60, 61] CA IX levels were significantly lower in CA IX-knockdown compared to CA IX-expressing tumors (Figures 3A & 3B). Additionally, as determined by immunofluorescence staining, membranous CA IX expression co-localized with the exogenous hypoxia marker pimonidazole in CA IX-expressing tumors, whereas in CA IX-knockdown tumor hypoxia, very low or no CA IX expression was present (Figure 3C). This confirms efficient CA IX knockdown and thus a CA IX-dependent uptake of [^{68}Ga]-**2**.

In order to determine the optimal imaging time point, μPET scans were acquired hourly from 1 to 4 h post injection (h p.i.) of [^{68}Ga]-**2**. Tumor uptake in the CA IX-expressing model was clearly observed and found to be highest at 1 h p.i. (Figure 4A). This time point was selected for all subsequent experiments. Additionally, it was found that the agent was rapidly excreted renally, as observed by the high presence of the agent in the kidneys and bladder. Mass spectrometry analysis of the urine confirmed the compound was cleared without metabolism.

To assess compound selectivity, uptake was compared between mice with either CA IX-expressing or CA IX-knockdown tumors. Although CA IX-knockdown tumors tend to grow

slower compared to their CA IX-expressing counterparts,[61] tumor volumes at time of scans were not statistically different (P = 0.422) between the two groups (315 ± 104 and 277 ± 63 mm^3 for CA IX-expressing and CA IX-knockdown tumors respectively). The TBR was significantly higher (P < 0.01) in mice bearing CA IX-expressing (3.87 ± 1.34) as compared to mice bearing CA IX-knockdown (1.99 ± 0.99) tumors (Figures 4B & 4C). Uptake of [^{68}Ga]-**2** was therefore found to be CA IX-dependent. However, lack of anatomical information in the acquired PET images prompted us to verify co-localisation with CT. Therefore experiments were repeated to include CT scans, enabling better tumor delineation in the fused PET/CT images and more clearly confirming the localization of the agent in the tumor. Again tumor volumes at time of scans were not statistically different (P = 0.071) between the two groups (492 ± 390 and 125 ± 44 mm^3 for CA IX-expressing and CA IX-knockdown tumors respectively). Similar to the first experiment, TBR was significantly higher (P < 0.01) in mice bearing CA IX-expressing (2.36 ± 0.424) tumors as compared to mice bearing CA IX-knockdown (1.30 ± 0.350) tumors (Figures 5A & 5B). Autoradiography analysis of tumor sections supported the μPET results, showing a higher signal intensity relative to injected dose (ID) in CA IX-expressing tumors (9.12×10^{-7} ± 7.25×10^{-7}) as compared to CA IX-knockdown (3.84×10^{-7} ± 1.53×10^{-7}) tumors (Figure 5C). Low uptake of [^{68}Ga]-**2** has been also observed in CA IX-knockdown model, which can be explained by residual CA IX expression in these tumors. Nevertheless, significantly higher uptake of [^{68}Ga]-**2** in tumors with high CA IX expression confirms selectivity of this imaging compound.

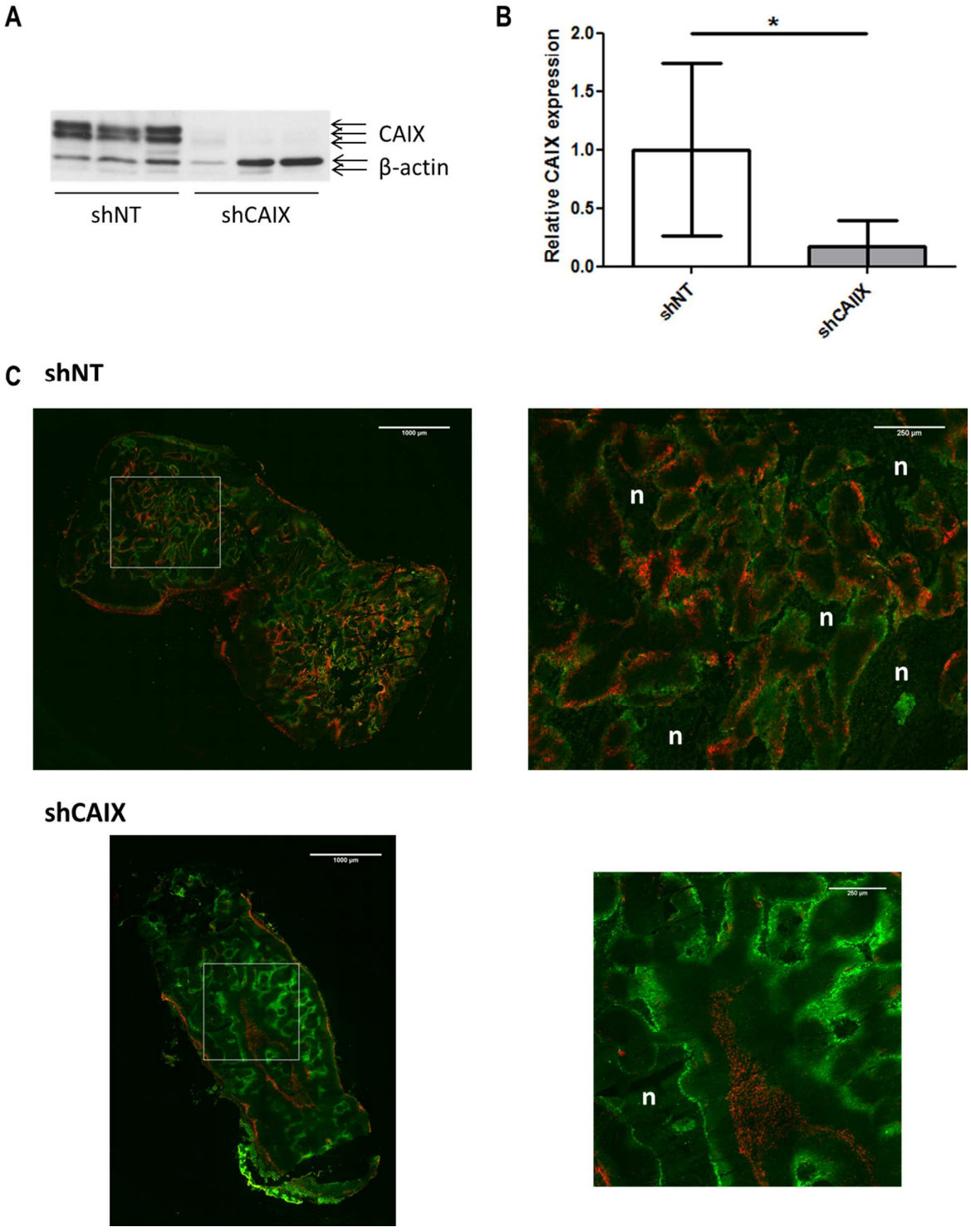

Figure 3. CA IX expression in mice bearing CA IX-expressing (shNT) or CA IX-knockdown (shCA IX) tumors. A) Western blot showing CA IX protein levels in representative samples. B) Quantification of CA IX protein levels as determined by Western blot for all shNT and

shCA IX tumors. C) Immunofluorescence staining of CA IX (red) and the hypoxia marker pimonidazole (green). Right-side images are magnifications of areas within the white rectangles in the left-side images. “n” indicates necrotic areas.

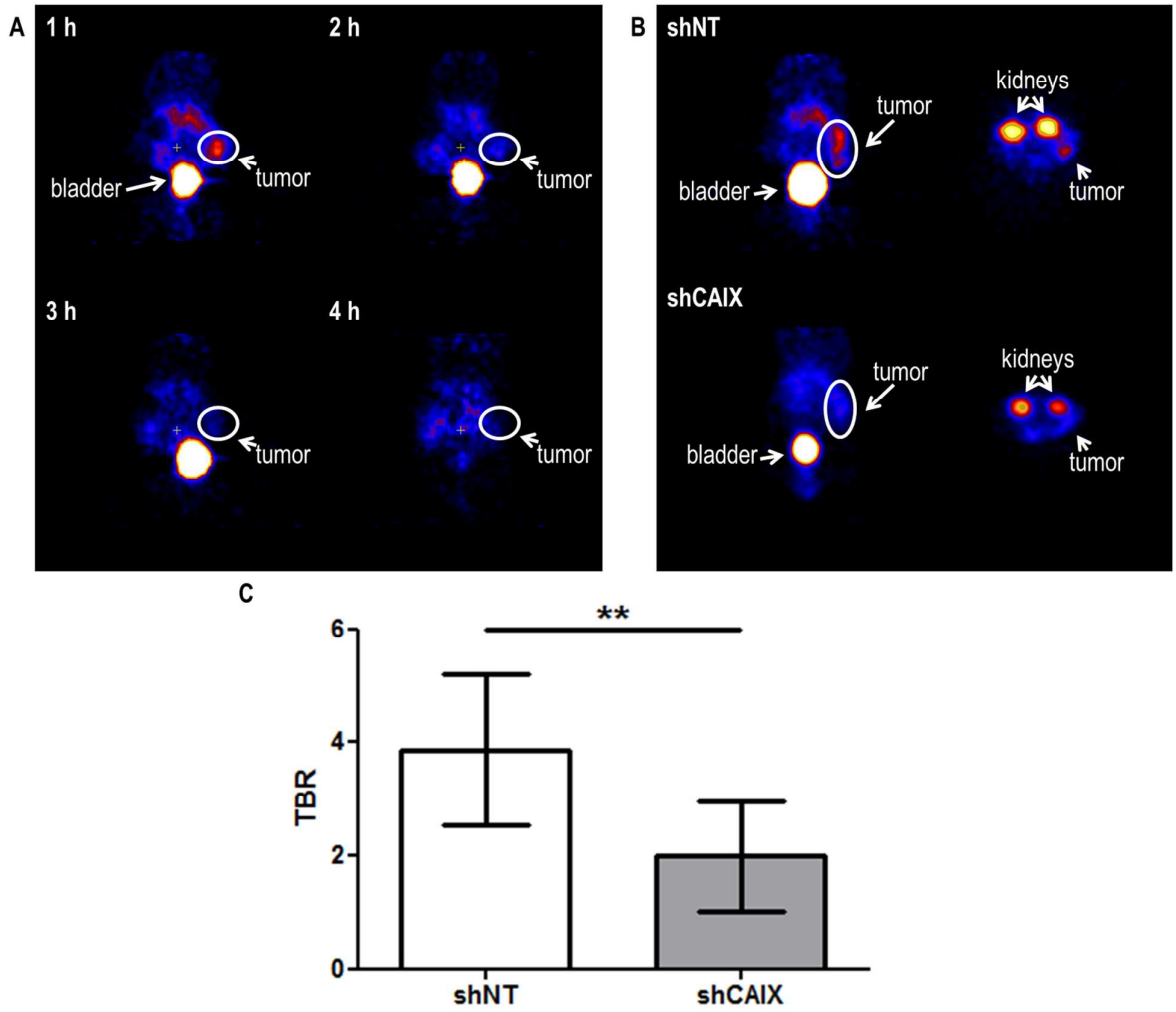

Figure 4. [^{68}Ga]-**2** uptake in mice bearing CA IX-expressing (shNT) or CA IX-knockdown (shCA IX) tumors. A) Representative µPET scans 1-4 h p.i. in a shNT-tumor bearing mouse. B) Representative µPET scans 1 h p.i. C) TBRs of [^{68}Ga]-**2** uptake determined from PET scans of shNT-tumor bearing mice (n = 11) and shCA IX-tumor bearing mice (n = 6). **P < 0.01.

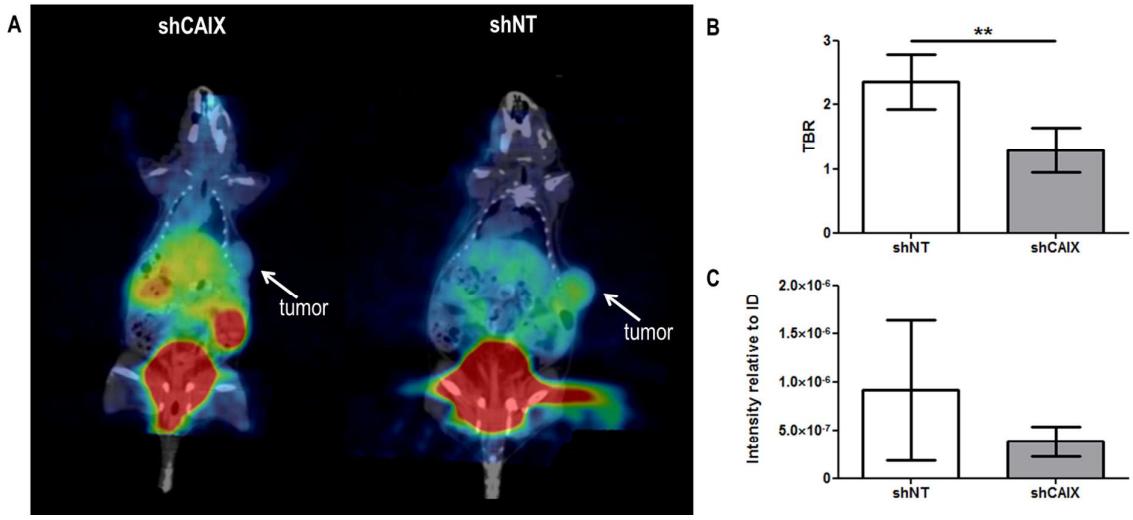

Figure 5: [^{68}Ga]-**2** uptake in mice bearing CA IX-expressing (shNT) or CA IX-knockdown (shCA IX) tumors. A) Representative µPET/CT fusion images 1 h p.i. B) TBRs of [^{68}Ga]-**2** uptake determined from PET scans of shNT-tumor bearing mice (n = 4) and shCA IX-tumor bearing mice (n = 5). ** $P < 0.01$. C) Signal intensity relative to injected dose (ID) as determined by autoradiography analysis on tumor sections from shNT-tumor bearing mice (n = 6) and shCA IX-tumor bearing mice (n = 6).

Conclusion

This study provides the first evidence of non-invasive, specific detection of CA IX in vivo, using a CA IX targeting small molecule PET radiotracer, [^{68}Ga]-**2**. The synthesis of the unlabeled precursor of [^{68}Ga]-**2** (compound **14**) and the radiochemistry to introduce ^{68}Ga was straightforward, proceeded in good yields and was reproducible while the biopharmaceutical properties were favorable. This study is a promising step towards a new predictive tool that will enable testing of the potential of CA IX expression as a biomarker for selection of patients eligible for CA IX-targeting anticancer therapies.

Experimental

Chemistry - General Methods and Synthesis

All starting materials and reagents were purchased from commercial suppliers. Where specified, solvents were available commercially dried or dried prior to use. Reactions took place open to the atmosphere unless otherwise specified. Reaction progress was monitored by: TLC using silica gel-60 F254 plates with detection by short wave UV fluorescence (λ = 254 nm) and staining with ninhydrin (1 g ninhydrin, 200 mL EtOH, 8mL acetic acid), $KMnO_4$ ($KMnO_4$ (0.75g), K_2CO_3 (5 g), NaOH (75 mg), H_2O (100 mL) or vanillin stain (5 g of vanillin in a mixture of EtOH:H_2O:H_2SO_4 = 87:10.2:2.8 with subsequent heating; by TLC using RP-18 silica gel-60 F254s plates with detection by short wave UV fluorescence; by high pressure liquid chromatography (HPLC) on an Agilent 1100 system using a Thermo Betasil C18 (150 × 4.6 mm, 5 μm) column. A gradient method was used of 95:5 → 5:95 H_2O (+ 0.1% TFA): Acetonitrile (+0.1% TFA) over 10 mins, 1 ml/min flow rate. Silica gel flash chromatography was performed using silica gel 60 Å (230−400 mesh). NMR (^{1}H, ^{13}C{^{1}H}, 1H-1H gCOSY, and HSQC) spectra were recorded on either a 400 or 500 MHz spectrometer at 30 °C. ^{1}H NMR spectra were referenced to the residual solvent peak ($CDCl_3$ δ 7.26 ppm, DMSO-d_6 δ 2.50 ppm). ^{13}C NMR spectra were referenced to the internal solvent ($CDCl_3$ δ 77.0 ppm, DMSO-d_6 δ 39.5 ppm). Multiplicity is indicated as follows: s (singlet), d (doublet), t (triplet), q (quaternary), qn (quintuplet), m (multiplet), dd (doublet of doublet), ddd (doublet of doublet of doublet), b (broad). Coupling constants (*J*) are reported in hertz (Hz). Mestrenova 6.1 software was used for NMR analysis. Melting points are uncorrected. Mass spectra (low and high resolution) were recorded using electrospray as the ionization technique in positive ion and/or negative ion modes as stated. Purity of all final compounds (**8**, **9**, ^{nat}Ga-**1** and ^{nat}Ga-**2**) was ≥ 95% as determined by HPLC with UV detection. Compounds **3**, **4**, **5, 7** and **10** were

synthesised as described elsewhere, with characterisation in agreement with literature.[53, 54, 56, 62-65] Numbering of DOTA compounds used for NMR assignments is shown below.

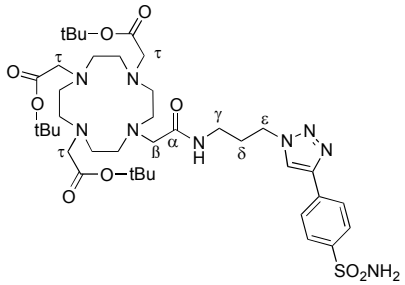

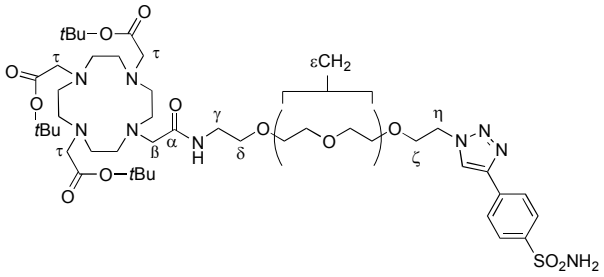

Synthesis methods

General Procedure 1: Synthesis of brominated [linker] components

The amino-azide precursor (1 equiv) was suspended in a biphasic DCM/NaOH (aq) solution (2:1, 2-3 equiv NaOH) and cooled to 0 °C. Bromoacetyl bromide (3 equiv) was added dropwise to the DCM layer. The solution was then stirred vigorously overnight at rt. The reaction mix was diluted with DCM and H_2O and the aqueous fraction extracted with DCM (2× 50 mL). The organic fractions were combined and washed with Na_2CO_3 (50 mM, 3×), dried with $MgSO_4$, filtered and concentrated. The crude compound was sufficiently pure and used crude in the next step.

General Procedure 2: Addition of "cold" Ga

The parent compound (**9** or **14**, 1 equiv) was suspended in H_2O and $Ga(NO_3)_3 \bullet xH_2O$ (aq) (excess) added. The pH of the reaction was adjusted to ~ pH 4.5 using KOH (1.0 M) or HCl (1.0 M). The reaction mixture was heated at 80 °C and the pH monitored and adjusted accordingly to maintain pH 4.5. The reaction mix stabilised after ~ 2 h. Reaction progress was monitored by LC-MS. Products were purified by RP-18 flash column chromatography

(H_2O/MeOH 100:0→5:95%) and the solvent was removed in vacuo leaving a hygroscopic solid.

***N*-(3-azidopropyl)-2-bromoacetamide (4)**. The title compound was synthesized from 3-azido-1-propanamine HCl salt (**3**) (1.5 g, 11 mmol) and NaOH (2 equiv) using general procedure 1 and isolated as a yellow oil (1.9 g, 78%). Rf 0.13 (90:10 DCM/MeOH). ^{1}H NMR (500 MHz, $CDCl_3$) δ_H 6.72 (br s, 1H, NH), 3.88 (s, 2H, βCH_2), 3.40-3.36 (m, 4H, γCH_2, εCH_2), 1.82 (quint, 2H, J = 6.60Hz, δCH_2). ^{13}C NMR (125 MHz, $CDCl_3$) 165.8 (αC=O), 49.5 (εCH_2 or γCH_2), 38.1 (εCH_2 or γCH_2), 29.3 (βCH_2), 28.6 (δCH_2). LRMS (ESI$^-$): m/z = 221, 219 [M–H; ^{81}Br, ^{79}Br]$^-$. HRMS (ESI)$^+$ Calcd for $C_5H_9{}^{79}BrN_4NaO^+$: 242.9852. Found: 242.9852. ^{1}H NMR was in agreement with the data reported in the literature.[62]

2-Bromo-*N*-(3-[4-(4-sulfamoylphenyl)-1*H*-1,2,3-triazol-1-yl]propyl)acetamide (6)

$CuSO_4$ (7 mg, 0.027 mmol) and sodium ascorbate (10.8 mg, 0.055 mmol) were combined in 1 mL H_2O and added to a solution of alkyne (**11**) (100 mg, 0.55 mmol), azide (**5**) (145 mg, 0.66 mmol) and TBTA (14.5 mg, 0.055 mmol) in DMSO (2 mL) and the mixture was left to stir at 45 °C and monitored by TLC. Once complete (1.5h), the reaction mixture was filtered through celite® and washed with H_2O and the filtrate redissolved in DMF. The DMF was concentrated to a minimum amount before EtOAc (30 mL) was added and the organic phase rapidly washed with EDTA in ammonium hydroxide (1.0 M, 50 mL). The organic fraction was dried ($MgSO_4$), filtered, and the remaining residue purified by flash column chromatography (90:10 EtOAc/MeOH). The product was isolated as a white powder (0.04 g, 18%). Rf 0.36 (80:20 DCM/MeOH), mp 182-185 °C. ^{1}H NMR (500 MHz, DMSO-d_6) δ_H 8.70 (s, 1H, triazole CH), 8.39 (t, 1H, NH), 8.02 (m, 2H, 2 × ArC*H*), 7.89 (m, 2H, 2 × ArC*H*), 7.37 (s, 2H, SO_2NH_2), 4.45 (t, J = 7.0 Hz, 2H, εCH_2), 3.85 (s, 2H, βCH_2), 3.15 (q, J = 6.7 Hz, 2H,

γCH_2), 2.08 – 2.02 (quint, *J* = 6.9 Hz, 2H, δCH_2). ^{13}C NMR (500 MHz, DMSO-d_6) δ_C 166.2 (αC=O), 145.0 (C*q*), 143.1 (triazole C*q*), 133.9 (C*q*), 126.4 (2 × CHAr), 125.3 (2 × CHAr), 122.6 (triazole CH), 47.4 (εCH2), 36.3 (γCH_2), 29.5 (βCH_2 and δCH_2), 29.4 (βCH_2 and δCH_2). LRMS (ESI$^-$): *m/z* = 402, 400 [M-H; ^{81}Br, ^{79}Br]$^-$. HRMS (ESI) Calcd for $C_{13}H_{16}BrN_5O_3S^+$: 402.0228. Found: 402.0208.

Tri-*tert*-butyl 2,2',2''-(10-(2-oxo-2-((3-(4-(4-sulfamoylphenyl)-1*H*-1,2,3-triazol-1-yl)propyl)amino)ethyl)-1,4,7,10-tetraazacyclododecane-1,4,7-triyl)triacetate (8)

Compound **7** (109 mg, 0.21 mmol), **6** (85 mg, 0.21 mmol) and K_2CO_3 (58 mg, 0.42 mmol) were dissolved in anhyd MeCN (5 mL) and the reaction mixture was stirred overnight at room temperature. The mixture was filtered through celite® and washed with MeOH. The residue was purified by flash column chromatography (gradient 100% DCM→ 85:15 DCM/MeOH). Appropriate fractions were collected together and the product was isolated as a hygroscopic solid (59.3 mg, 33%). Rf 0.04 (95:5 DCM:MeOH). ^{1}H NMR (400 MHz, DMSO-d_6, 85 °C) δ_H 8.63 (s, 1H, CH triazole), 8.17 (t, *J* = 5.38 Hz, 1H, NH), 7.98 (m, 2H, 2 × ArCH), 7.91 (m, 2H, 2 × ArCH), 7.20 (s, 2H, SO_2NH_2), 4.45 (t, *J* = 7.1 Hz, 2H, εCH_2), 3.53 (MeOH), 3.19 (m, 2H, γCH_2), 3.08 (s, 6H, τCH_2), 2.94 (dt, *J* = 42.0, 5.2 Hz, 2H, CH_2 Aza), 2.61 (br, 7H, CH_2 Aza), 2.30 (br, 7H, CH_2 Aza), 2.10 (quint, *J* = 6.9 Hz, 2H, δCH_2), 1.44 (s, 9H, *t*Bu), 1.40 (s, 18H, 2 × *t*Bu). ^{13}C NMR (75.5 MHz, DMSO-d_6) δ_C 172.5 (C=O), 172.2 (2 × C=O), 171.6 (C=O), 145.0 (C*q* triazole), 143.1 (C*q* Ar), 133.9 (C*q* Ar), 126.4 (2 × ArCH), 125.3 (2 × ArCH), 122.5 (CH triazole), 81.1 (C*q* *t*Bu), 80.9 (2 × C*q* *t*Bu), 69.8(MeOH), 60.18 (τCH_2), 55.7 (τCH_2), 55.3 (τCH_2), 54-49 - CH_2 Aza in baseline, 47.6 (εCH_2), 36.0 (γCH_2), 29.6 (δCH_2), 27.9 (βCH_3), 27.5 (CH_3 *t*Bu). LRMS (ESI$^+$): *m/z* = 836 [M+H]$^+$. HRMS (ESI) Calcd for $C_{39}H_{65}N_9NaO_9S^+$:858.4518. Found: 858.4513.

2,2',2''-(10-(2-Oxo-2-((3-(4-(4-sulfamoylphenyl)-1*H*-1,2,3-triazol-1-yl)propyl)amino)ethyl)-1,4,7,10-tetraazacyclododecane-1,4,7-triyl)triacetic acid (9)

Compound **8** (87.7 mg, 0.1 mmol) was dissolved in DCM/TFA (1:1) (8 mL) and stirred at 40 °C for 3 h. Reaction progress was monitored by LC-MS and RP-18 TLC and conversion was complete. The solvent was removed *in vacuo* and then co-evaporated with water (×3) followed by lyophilization. Rf 0.76 (50:50 MeOH/H_2O RP-18 TLC). Samples for radiolabelling were purified using HPLC (isocratic 7:93 MeCN:H_2O + 0.1% Formic acid – Waters Atlantis® T3 C18, 19 × 150 mm, 10 μM at a flowrate of 12 mL/min). Product fractions were collected and the solvent removed in vacuo (8.5mg, 52% HPLC recovery). ^{1}H NMR (500 MHz, DMSO-d_6) δ_H 8.69 (s, 1H, CH triazole), 8.57 (t, J = 5.2 Hz, 1H, NH), 8.01 (m, 2H, 2 × ArCH), 7.90 (s, 2H, 2 × ArCH), 7.38 (s, 2H, SO_2NH_2), 4.48 (t, J = 6.8 Hz, 2H, εCH_2), 4.1-3.0 (m, signals masked by broad H_2O peak), 3.18 (q, J = 5.1 Hz, 2H, γCH_2), 2.08 (quint, 2H, δCH_2). Correlations under the H_2O peak were observed in the ^{1}H-^{1}H gCOSY, and HSQC spectra. LRMS (ESI$^+$): *m/z* = 668 $[M+H]^+$. HRMS (ESI) Calcd for $C_{27}H_{42}N_9O_9S^+$: 668.2821. Found: 668.2819.

***N*-[2-[2-[2-(2-Azidoethoxy)ethoxy]ethoxy]ethyl]-2-bromoacetamide (11)**. The title compound was synthesized from 11-azido-3,6,9-trioxaundecanamine (**10**) (450 mg, 2.08 mmol) using general procedure 1 and isolated as a yellow oil (0.54 g, 76%). Rf 0.35 (95:5 DCM/MeOH). ^{1}H NMR (500 MHz, $CDCl_3$) δ_H 6.92 (s, 1H, NH), 3.87 (s, 2H, βCH_2), 3.71 – 3.63 (m, 10H, εCH_2, ζCH_2), 3.59 (t, J = 5.1 Hz, 2H, δCH_2), 3.49 (m, 2H, γCH_2), 3.39 (t, J = 5.0 Hz, 2H, ηCH_2N_3). ^{13}C NMR (125 MHz, $CDCl_3$) 165.8 (αC=O), (70.9, 70.8, 70.7, 70.5, 70.2, εCH, ζCH_2), 69.5 (δCH_2), 50.8 (ηCH_2), 40.1 (γCH_2), 29.2 (βCH_2). LRMS (ESI$^-$): *m/z* 339, 337 [M-H, ^{81}Br, ^{79}Br]$^-$. HRMS (ESI$^+$) Calcd for $C_{10}H_{19}{}^{79}BrN_4O_4^+$: 339.0662. Found: 339.0684. ^{1}H NMR was in agreement with the data reported in the literature.[66]

2-Bromo-*N*-[[2-(2-[2-[4-(4-sulfamoylphenyl)-1*H*-1,2,3-triazol-1-yl]ethoxy]ethoxy) ethoxy]methyl]acetamide (12)

$CuSO_4$ (2 mg, 0.007 mmol) and sodium ascorbate (14 mg, 0.071 mmol) were combined in 1 mL H_2O and added to a solution of azide (**11**) (264 mg, 0.78 mmol), alkyne (**5**) (128 mg, 0.71 mmol) and TBTA (4 mg, 0.007 mmol) in DMSO (2 mL) and the mixture was left to stir at 45 °C and monitored by TLC. Once complete, the reaction mixture was diluted with H_2O and EtOAc and the aqueous phase extracted with EtOAc (4× 30 mL). The organic fractions were combined and washed with EDTA (1.0 M) in ammonium hydroxide (28.0-30.0%, NH3 basis) solution, dried (Na_2SO_4), filtered and purified by flash column chromatography (95:5 EtOAc/MeOH or DCM/MeOH). The product was isolated as a yellow gum (0.148g, 40%). Rf 0.2 (95:5 DCM/MeOH), mp 85-90 °C. ^{1}H NMR (500 MHz, DMSO-d_6) δ_H 8.66 (s, 1H, triazole CH), 8.28 (br t, J = 5.90 Hz 1H, NH), 8.02 (m, 2H, 2 × ArCH), 7.90 (m, 2H, 2 × ArCH), 7.36 (s, 2H, SO_2NH_2), 4.60 (t, J = 5.2 Hz, 2H, ηCH_2), 3.88 (t, J = 5.2 Hz, 2H, ζCH_2), 3.84 (s, 2H, βCH_2), 3.58 – 3.45 (m, 8H, εCH_2), 3.39 (t, J = 5.7 Hz, 2H, δCH_2NH), 3.20 (q, J = 5.67 Hz, 2H, γCH_2). ^{13}C NMR (500 MHz, DMSO-d_6) δ_C 166.0 (αC=O), 144.9 (C*q* Ar-trizole), 143.0 (C*q* Ar-SO_2NH_2), 133.9 (C*q* triazole), 126.3 (2 × ArCH), 125.25 (2 × ArCH), 122.84 (CH triazole), 69.7-69.5 (εCH_2, 4C), 68.7 (δCH_2 or ζCH_2), 68.6 (δCH_2 or ζCH_2), 54.8 (DCM), 49.7 (ηCH_2), 48.6 (γCH_2), 29.4 (βCH_2). LRMS (ESI$^+$): *m/z* = 544, 542 [M+Na; ^{81}Br, ^{79}Br]$^+$; 522, 520 [M+H; ^{81}Br, ^{79}Br]$^+$. HRMS (ESI) Calcd for $C_{18}H_{26}{}^{79}BrN_5NaO_6S^+$: 542.0679. Found: 542.0681.

Tri-*tert*-butyl 2,2',2''-(10-(2-oxo-14-(4-(4-sulfamoylphenyl)-1*H*-1,2,3-triazol-1-yl)-6,9,12-trioxa-3-azatetradecyl)-1,4,7,10-tetraazacyclododecane-1,4,7-triyl)triacetate (13)

Compound **12** (0.196 g, 0.37 mmol), **7** (253 mg, 0.49 mmol) and K_2CO_3 (68 mg, 0.49 mmol) were dissolved in anh MeCN (8 mL) and stirred at 60 °C for 3h. The reaction mixture was filtered through celite® and washed (MeCN), concentrated and the remaining residue purified by column chromatography (90:10 DCM: MeOH). Fractions were monitored by HPLC and positive fractions combined to give the title compound as a hygroscopic off-white solid (0.268 g, 76%). Rf 0.28 (90:10 DCM/MeOH). ^{1}H NMR (500 MHz, DMSO-d_6) δ_H 8.67 (s, 1H, CH triazole), 8.18 (t, J = 5.9 Hz, 1H, NH), 8.02 (m, 2H, 2 × ArCH), 7.90 (m, 2H, 2 × ArCH), 7.37 (s, 2H, SO_2NH_2), 4.59 (t, J = 5.1 Hz, 2H, ηCH$_2$), 3.88 (t, J = 5.1 Hz, 2H, ζCH$_2$), 3.50 (m, 8H, εCH$_2$), 3.41 (t, J = 5.94 Hz, 2H, δCH$_2$), 3.21 (m, 2H, γCH$_2$), 3.1 - 2.0 (br, m, 24H, Aza CH$_2$, βCH$_2$, 3 × τCH$_2$), 1.43 (s, 9H, *t*Bu), 1.41 (s, 18H, 2 × *t*Bu). ^{13}C NMR (125 MHz, DMSO-d_6) δ_C 172.5 (C=O), 172.1 (2 × C=O), 171.6 (C=O), 144.9 (C*q* triazole), 143.1 (C*q* Ar), 134.0 (C*q* Ar), 126.3 (2 × ArCH), 125.2 (2 × ArCH), 122.8 (CH triazole), 81.1 (C*q* *t*Bu), 80.9 (2× C*q* *t*Bu), 69.6 -69.5 (εCH$_2$, βCH$_2$), 68.8 (ζCH$_2$), 68.5 (δCH$_2$), 59.7 (τCH$_2$), 55.7 (τCH$_2$), 55.3 (τCH$_2$), 49.7 (ηCH$_2$), 38.5 (γCH$_2$), 27.5 (CH$_3$ *t*Bu), CH$_2$ Aza peaks masked in baseline. LRMS (ESI$^+$): *m/z* = 954 [M+H]$^+$. HRMS (ESI) Calcd for $C_{44}H_{75}N_9NaO_{12}S^+$: 976.5148. Found: 976.5155.

2-[4,10-Bis(carboxymethyl)-7-[[[2-[2-(2-[2-[4-(4-sulfamoylphenyl)-1*H*-1,2,3-triazol-1-yl]ethoxy]ethoxy)ethoxy]ethyl]carbamoyl]methyl]1,4,7,10 tetraazacyclododecan-1-yl]acetic acid (14).

Compound **13** (0.219 mg, 0.23 mmol) was dissolved in formic acid (10 mL) or TFA/DCM (1:1) and stirred at 60 °C. The reaction was monitored by HPLC. On completion, water (10 mL) was added and then the solvent removed in vacuo and then co-evaporated with water (×3) followed by lyophilization. The sample was purified by reverse phase column chromatography using a gradient of 100% H_2O → 95:5 MeOH:H_2O and the product isolated

as a hygroscopic white gum (144 mg, 80%). Rf 0.53 (50:50 MeOH:H_2O RP-18 TLC). Samples were further purified via HPLC prior to radiolabelling (Isocratic 10:90 MeCN: H_2O +0.1% Formic acid – Waters Atlantis® T3 C18, 19 × 150 mm, 10 μm, at a flowrate of 12 mL/min). Product fractions were collected and solvent removed in vacuo (19%). ^{1}H NMR (500 MHz, DMSO-d_6) δ_H 8.67 (s, 1H, CH triazole), 8.17 (br, 1H, NH), 8.02 (m, 2H, 2 × ArCH), 7.90 (m, 2H, 2 × ArCH), 7.38 (s, 2H, SO_2NH_2), 4.60 (t, J = 5.0 Hz, 2H, ηCH$_2$), 3.88 (t, J = 5.3 Hz, 2H, ζCH$_2$), the remaining signals were masked by broad H_2O peak. Correlations were observed in the ^{1}H-^{1}H gCOSY, and HSQC spectra. LRMS (ESI$^+$): *m/z* 786 [M+H]$^+$. HRMS (ESI) Calcd for $C_{32}H_{51}N_9NaO_{12}S^+$: 808.3281. Found: 808.3278.

2,2',2''-(10-(2-Oxo-2-((3-(4-(4-sulfamoylphenyl)-1*H*-1,2,3-triazol-1-yl)propyl)amino)ethyl)-1,4,7,10-tetraazacyclododecane-1,4,7-triyl)triacetic acid Gallium complex (^{nat}Ga-1)

Compound **9** (48 mg, 0.071 mmol) was treated as per general procedure **2** to give the title compound as a hygroscopic white solid. LRMS (ESI$^-$): *m/z* = 734 [M-H]$^-$. HRMS (ESI) Calcd for $C_{27}H_{38}GaN_9NaO_9S^+$:756.1661. Found: 756.1660.

2-[4,10-Bis(carboxymethyl)-7-[([2-[2-(2-[2-[4-(4-sulfamoylphenyl)-1*H*-1,2,3-triazol-1-yl]ethoxy]ethoxy)ethoxy]ethyl]carbamoyl]methyl]1,4,7,10 tetraazacyclododecan-1-yl]acetic acid Gallium complex (^{nat}Ga-2).

Compound **14** (50 mg, 0.064 mmol) was treated as per general procedure 2 to give the title compound as a hygroscopic white solid. Rf 0.65 (RP-18TLC 60:40 H_2O/MeOH). LRMS (ESI$^+$): *m/z* 852 [M+H]$^+$. HRMS (ESI) Calcd for $C_{32}H_{49}GaN_9O_{12}S^+$: 852.2472. Found: 852.2460.

Cell culture

Human MDA-MB-231 breast cancer cells (ATCC®-26™) for toxicity studies were cultured in Roswell Park Memorial Institute medium (RPMI)-1640 media supplemented with 10% Fetal Bovine Serum (FBS), 100 U/mL penicillin and 100 µg/mL streptomycin at 37 °C and 5% CO_2. Cells were seeded at 3×10^4 cells/well (200 µL, RPMI-1640) and allowed to grow for 24 h before being exposed to the compound of interest. Untreated cells were used as a control. HCT116 human colorectal carcinoma cells (ATCC® CCL-247™) stably expressing a CA IX-targeting shRNA (shCA IX) or non-targeting shRNA (shNT) construct established as described previously[61], were routinely cultured in Dulbecco's Modified Eagle's Medium (DMEM) supplemented with 10% FBS at 37 °C.

Cell proliferation assay

Compounds were dissolved in RPMI media to a final concentration of 1 mM and linear dilutions ranging from 1 mM – 1 µM were carried out in culture medium. After 24 h of treatment at 37 °C, 5% CO_2, MTT (20 µL, 5 mg/mL) was added. After 3 hours, SDS (50 µL, 20% (w/v) SDS in 0.01M HCl) was added and the plates left overnight before being read by a SpectraMax fluorescence plate reader (Molecular Devices) at 570 nm. Experiments were performed in triplicate and where possible, were repeated three times. Values were determined using the Graphpad prism software.

Radiolabelling

Radiolabelling with ^{67}Ga

[^{67}Ga]$GaCl_3$ in 0.1 M HCl was prepared from commercial [^{67}Ga]citrate for injection (Lantheus) via standard conversion methods.[67] To an acid washed microcentrifuge tube, the DOTA complex (25 µL, 1 mM H_2O) and sodium acetate buffer (100 µL, 0.1 M, pH 4.3) were

combined and the solution agitated. $^{67}GaCl_3$ (18-21 MBq in 0.1M HCl) was added and the solution heated at 95 °C for 10 mins using a solid state heating block. The sample was stirred via convection. Once complete, a sample (20 µL, ~3 MBq) was analysed by HPLC and the radiochemical purity noted. Solutions were purified by HPLC (Atlantis® T3, 10 × 250 mm, 5 µM, flow rate 3 ml/min) (or rapid reverse phase C-18 solid phase extraction (SPE, washed with copious amounts of H_2O and compounds eluted in 50:50 EtOH:H_2O).

[^{67}Ga]-1 and [^{67}Ga]-2 Stability versus Human serum

Human serum (150 µL), was placed in a previously acid washed 0.5 mL microcentrifuge tube. To this was added 10× PBS concentrate (15 µL), water (60 µL) and the radio-complex (75 µL in water, 0.24 -0.28 MBq). The mixture was agitated via a bench vortex mixer and then incubated at 37.5 °C for the course of the study. Aliquots (5 -15 µL) were injected onto a Phenomenex Biosep SEC-S 3000 column (300mm × 7.8 mm ID, 5 µm, pore size 290 Å), with a mobile phase of 50 mM sodium phosphate, 300 mM NaCl, pH 7.0, 0.2 µm filtered) at 1 mL/min on a HPLC system. Serum uptake was assessed as a percentage of the total activity in chromatogram.

[^{67}Ga]-1 and [^{67}Ga]-2 Stability in Phosphate buffered saline

10× PBS concentrate (20 µL), water (160 µL) and the radio-complex (20 µL in water, 0.2 - 0.23 MBq) were added together in a previously acid washed 0.5 mL microcentrifuge tube. The solution was agitated and then incubated at 37.5 °C for the course of the study. Aliquots (5 -50 µL) were injected onto a Waters Atlantis® T3 C18 column (150 mm × 4.6mm I.D., 3 µm), with a mobile phase of MeCN/ammonium formate buffer (120 mM, pH 4.43, 0.2 µm filtered) (16:84) at 0.6 mL/min on a HPLC system. Stability was assessed as a percentage of parent radio-complex.

Radiolabelling with ^{68}Ga

Reaction progress was monitored by radio-HPLC equipped with an Inertsil ODS C18, 5 μM, 4.6 × 250 mm column using a gradient method (100% H_2O → 100% MeCN over 17 mins, 1 ml/min). Sodium acetate or ammonium acetate buffer (3 M, 400 μL, pH 4.3-4.5) combined with ~800 MBq ^{68}Ga in aqueous HCl (0.6M, ~1.2 mL) which was eluted from an iThemba 1480 MBq ^{68}Ge/^{68}Ga generator. Compound **14** in H_2O (40 μL, 1 mM) was added and the solution was mixed by Eppendorf pipette (pH ~4.5) then heated at 99 °C for 10 mins. Reaction mixtures were analysed by radio-HPLC and radiochemical purity was consistently >95%. The specific activity of [^{68}Ga]-**2** at the time of radiolabelling was ~20 MBq/nmol (800 MBq/40nmole). Small animal imaging PET studies with [^{68}Ga]-**2** were carried out between 1-2.5 h post radiolabelling of **14** →[^{68}Ga]-**2**. No further purification was carried out prior to imaging. Samples (~3.7 MBq) were diluted in 0.9% saline solution prior to injection.

CA Inhibition Assay

An Applied Photophysics stopped-flow instrument was used for assaying the CA-catalyzed CO_2 hydration activity.[58] IC_{50} values were obtained from dose response curves working at seven different concentrations of test compound by fitting the curves using PRISM (www.graphpad.com) and non-linear least squares methods; values represent the mean of at least three different determinations as described previously.[39] The inhibition constants (K_i) were then derived by using the Cheng−Prusoff equation as follows: $K_i = IC_{50}/(1 + [S]/K_m)$, where [S] represents the CO_2 concentration at which the measurement was carried out and K_m the concentration of substrate at which the enzyme activity is at half maximal. All enzymes used were recombinant, produced in Escherichia coli as reported earlier.[68, 69] The

concentrations of enzymes used in the assay were: hCA I, 10.4 nM; hCA II, 8.3 nM; hCA IX, 8.0 nM; hCA XII, 12.4 nM.

Animal model

Animal experiments were performed using adult NMRI-*nu* mice. Animal facilities and experiments were in accordance with local institutional guidelines for animal welfare and were approved by the Maastricht University Animal Ethical Committee (number 2014-020). HCT116 cells stably expressing either a CA IX-targeting shRNA (shCA IX) (n=10) or non-targeting shRNA (shNT) (n=10) construct established as described previously[61] were resuspended in BD Matrigel™ Basement Membrane Matrix (BD Biosciences) and injected (10^6) subcutaneously into the lateral flank of the animal.

Image acquisition

Once tumors reached a volume between 180-300 mm^3, animals were intravenously (i.v.) injected via the lateral tail vein with ~3.7 MBq of the ^{68}Ga labelled sulfonamide compound diluted in 0.9% saline solution via an IV line flushed with 10% heparin saline solution. For PET and CT scans, animals receiving only a PET scan were anesthetized with isoflurane (induction 4%, maintenance 1-2%); animals receiving both PET and CT scans were anesthetized with an intraperitoneal injection of a 100 mg/kg ketamine / 10 mg/kg xylazine mixture. PET image acquisition was performed using a Focus 120 microPET (Siemens Medical Solutions USA, Inc.). Animals receiving only a PET scan underwent a 9 min emission scan 1, 2, 3 and 4 h post injection (p.i.), animals receiving both PET and CT scans a 15 min emission scan 1 h p.i. The OSEM-3D reconstructed PET images were viewed and analyzed using the PMOD software (PMOD Technologies Ltd). Activity data (Bq/mL) was

obtained by manually delineating Volumes Of Interest (VOIs) in the PET images for mice that received only a PET scan, or in the fused PET/CT images for mice that received both PET and CT scans, using the PMOD software. The tumor itself was delineated as tumor VOI (T), whereas the heart outflow area was delineated as blood VOI (B). Standardized Uptake Values (SUVs) were calculated by correcting activity data for ^{68}Ga injected dose, decay toward injection time, and weight of the animal. Data was quantified by calculating the T/B activity ratios (TBRs). CT image acquisition was performed using the SmART system (X-RAD 225CX; Precision X-Ray, North Branford, USA). Tumor volume at time of scanning was determined by delineating the tumor on the CT image using the PMOD software.

Western Blot

Samples from tumors were minced and proteins were isolated using RIPA buffer completed with a protease inhibitor cocktail (complete EDTA-free; Roche). Bradford assay (BioRad) was performed for protein quantification. Proteins were separated on a 10% SDS-PAGE gel and blotted onto a nitrocellulose membrane (GE Healthcare) by electrotransfer. Membranes were blocked in 5% non-fat dry milk and probed overnight with mouse anti-CA IX monoclonal antibody (M75, kindly provided by S. Pastorekova, Institute of Virology, Slovak Academy of Science, Bratislava, Slovak Republic) and mouse anti-β-actin monoclonal antibody (Cell Signaling). Subsequently membranes were probed with HRP-linked horse anti-mouse IgG antibodies (Cell Signaling), which were detected with Western blot detection reagents (Thermo Fisher Scientific).

Immunofluorescence

1 h before sacrifice, mice were injected intravenously with the hypoxia marker pimonidazole. After sacrifice, tumors were collected and sections were made. Sections were fixed with cold

acetone and non-specific binding was blocked using 1% normal goat serum at RT for 30 min. Sections were incubated overnight at 4°C with rabbit anti-CA IX polyclonal antibody (1:1000, Novus Biologicals) and FITC-conjugated mouse anti-pimonidazole monoclonal antibody (1:100, Hypoxyprobe, Bioconnect). Subsequently sections were incubated at RT for 1 h with Alexa Fluor® 594 conjugated goat anti-rabbit secondary antibody (1:500, Invitrogen). Mounting was done using Fluorescence mounting medium (Dako).

Autoradiography

Tumor sections (30 µm) were made using a cyrotome (Leica) and placed on high resolution phosphorimaging plates (Storage Phosphor Screen BAS-IP SR 2040 E Super Resolution, GE Healthcare) overnight. Plates were read using a Typhoon FLA 7000 laser scanner (GE Healthcare). Signal intensities were determined using the ImageQuant TL software (GE Healthcare), and normalized per animal to the respective ID.

Statistics

All statistical analyses were performed using the GraphPad Prism® version 5.03 software (GraphPad Software). Unpaired Student's t-test was used to determine the statistical significance of differences between two independent groups of variables.

Supporting Information. ^{1}H and ^{13}C NMR spectra for compounds and radiotraces are available free of charge via the Internet at http://pubs.acs.org.

Corresponding author

S.-A.P. Telephone: +61 7 3735 7825; e-mail: s.poulsen@griffith.edu.au.

L.D. Telephone: +31 43 388 2909; email: ludwig.dubois@maastrichtuniversity.nl

Keywords

hypoxia, oncology, CA IX, imaging, sulfonamide, triazole, PET

Acknowledgements

This work was funded by the Cancer Council Queensland (Project No. APP1058222) and the Australian Institute of Nuclear Science and Engineering (AINSE) (Project nos. ALNGRA15021 and ALNGRA13520). We thank the Australian Research Council (FT10100185 to S-AP). Authors acknowledge financial support from the Dutch Cancer Society (KWF UM 2012-5394 and KWF MAC 2013-6089). HCT116 human colorectal carcinoma cells (ATCC® CCL-247™) stably expressing a CA IX-targeting shRNA (shCA IX) or non-targeting shRNA (shNT) construct was kindly provided by Adrian Harris of the Weatherall Institute of Molecular Medicine, University of Oxford, John Radcliffe Hospital, Oxford, UK.

Abbreviations used

CA, carbonic anhydrase; $CDCl_3$, deuterated chloroform; Clint, intrinsic clearance value; CT, computed tomography; CuAAC, copper catalyzed azide alkyne cycloaddition; DOTA, 1,4,7,10-tetraazacyclododecane-N, N^{I} ,N^{II}, N^{III}-1,4,7,10-tetraacetic acid; DIPEA, diisopropylethylamine; DMEM, Dulbecco's Modified Eagle's Medium; DTPA, diethylenetriaminepentaacetic acid; E_H, predicted in vivo hepatic extraction ratio; FBS, Fetal Bovine Serum; FDA, United States Food and Drug Administration; Hb hemoglobin; h p.i,

hour post-injection; ID, injected dose; ITLC-SC, silica gel instant thin layer chromatography; LRMS, low resolution mass spectrometry; MeOH, methanol; MTT, (3-(4,5-dimethylthiazol-2-yl)-2,5-diphenyl tetrazolium bromide); Papp, membrane permeability; p.i., post injection; RCP, radiochemical purity; RP-HPLC, reverse phase high pressure liquid chromatography; RIPA, Radioimmunoprecipitation assay; RPMI, Roswell Park Memorial Institute; shCA IX, CA IX knockdown tumor; shNT, CA IX expressing tumor; SPE, solid phase extraction; SPECT, single photon emission computed tomography; $t_{1/2}$, half-life; TBR, tumor-to-blood; TBM, tumor-to-muscle; TBTA, tris(benzyltriazolylmethyl)amine.

References

1. Hanahan, D.; Weinberg, Robert A. Hallmarks of Cancer: The Next Generation. *Cell* **2011**, *144*, 646-674.

2. Horsman, M. R.; Mortensen, L. S.; Petersen, J. B.; Busk, M.; Overgaard, J. Imaging hypoxia to improve radiotherapy outcome. *Nat. Rev. Clin. Oncol.* **2012**, *9*, 674-687.

3. Rockwell, S.; Dobrucki, I. T.; Kim, E. Y.; Marrison, S. T.; Vu, V. T. Hypoxia and radiation therapy: Past history, ongoing research, and future promise. *Curr. Mol. Med.* **2009**, *9*, 442-458.

4. Peeters, S. G. J. A.; Zegers, C. M. L.; Biemans, R.; Lieuwes, N. G.; van Stiphout, R. G. P. M.; Yaromina, A.; Sun, J. D.; Hart, C. P.; Windhorst, A. D.; van Elmpt, W.; Dubois, L. J.; Lambin, P. TH-302 in Combination with Radiotherapy Enhances the Therapeutic Outcome and Is Associated with Pretreatment [18F]HX4 Hypoxia PET Imaging. *Clin. Cancer Res.* **2015**, *21*, 2984-2992.

5. Peeters, S. G. J. A.; Zegers, C. M. L.; Lieuwes, N. G.; van Elmpt, W.; Eriksson, J.; van Dongen, G. A. M. S.; Dubois, L.; Lambin, P. A Comparative Study of the Hypoxia PET Tracers [18F]HX4, [18F]FAZA, and [18F]FMISO in a Preclinical Tumor Model. *Int. J. Radiation Oncol. Biol. Phys.* **2015**, *91*, 351-359.

6. Zegers, C. M. L.; van Elmpt, W.; Reymen, B.; Even, A. J. G.; Troost, E. G. C.; Öllers, M. C.; Hoebers, F. J. P.; Houben, R. M. A.; Eriksson, J.; Windhorst, A. D.; Mottaghy, F. M.; De Ruysscher,

D.; Lambin, P. In Vivo Quantification of Hypoxic and Metabolic Status of NSCLC Tumors Using [18F]HX4 and [18F]FDG-PET/CT Imaging. *Clin. Cancer Res.* **2014**, *20*, 6389-6397.

7. Zegers, C. M. L.; Elmpt, W.; Szardenings, K.; Kolb, H.; Waxman, A.; Subramaniam, R. M.; Moon, D. H.; Brunetti, J. C.; Srinivas, S. M.; Lambin, P.; Chien, D. Repeatability of hypoxia PET imaging using [18F]HX4 in lung and head and neck cancer patients: a prospective multicenter trial. *Eur. J. Nucl. Med. Mol. Imaging,* **2015**, *42*, 1840-1849.

8. Loon, J.; Janssen, M. H. M.; Öllers, M.; Aerts, H. J. W. L.; Dubois, L.; Hochstenbag, M.; Dingemans, A.-M. C.; Lalisang, R.; Brans, B.; Windhorst, B.; Dongen, G. A.; Kolb, H.; Zhang, J.; Ruysscher, D.; Lambin, P. PET imaging of hypoxia using [18F]HX4: a phase I trial. *Eur. J. Nucl. Med. Mol. Imaging,* **2010**, *37*, 1663-1668.

9. Greer, S. N.; Metcalf, J. L.; Wang, Y.; Ohh, M. The updated biology of hypoxia-inducible factor. *EMBO J.* **2012**, *31*, 2448-2460.

10. Potter, C. P. S.; Harris, A. L. Diagnostic, prognostic and therapeutic implications of carbonic anhydrases in cancer. *Brit. J. Cancer* **2003**, *89*, 2-7.

11. Kaluz, S.; Kaluzová, M.; Liao, S.-Y.; Lerman, M.; Stanbridge, E. J. Transcriptional control of the tumor- and hypoxia-marker carbonic anhydrase 9: A one transcription factor (HIF-1) show? *BBA-Rev. Cancer,* **2009**, *1795*, 162-172.

12. Bao, B.; Groves, K.; Zhang, J.; Handy, E.; Kennedy, P.; Cuneo, G.; Supuran, C. T.; Yared, W.; Rajopadhye, M.; Peterson, J. D. *In Vivo* Imaging and Quantification of Carbonic Anhydrase IX Expression as an Endogenous Biomarker of Tumor Hypoxia. *PLoS ONE,* **2012**, *7*, e50860.

13. Potter, C.; Harris, A. L. Hypoxia inducible carbonic anhydrase IX, marker of tumour: hypoxia, survival pathway and therapy target. *Cell Cycle* **2003**, *3*, 159-162.

14. van Kuijk, S. J. A.; Yaromina, A.; Houben, R.; Niemans, R.; Lambin, P.; Dubois, L. J. Prognostic significance of carbonic anhydrase IX expression in cancer patients: A meta-analysis. *Front. Oncol.* **2016**, *6*, 69, 1-16

15. Neri, D.; Supuran, C. T. Interfering with pH regulation in tumours as a therapeutic strategy. *Nat. Rev. Drug Discov.* **2011**, *10*, 767-777.

16. Lawrentschuk, N.; Lee, F. T.; Jones, G.; Rigopoulos, A.; Mountain, A.; O'Keefe, G.; Papenfuss, A. T.; Bolton, D. M.; Davis, I. D.; Scott, A. M. Investigation of hypoxia and carbonic anhydrase IX expression in a renal cell carcinoma xenograft model with oxygen tension measurements and 124I-cG250 PET/CT. *Urol. Oncol-Semin. Ori.* **2011**, *29*, 411-420.

17. Carlin, S.; Khan, N.; Ku, T.; Longo, V. A.; Larson, S. M.; Smith-Jones, P. M. Molecular Targeting of Carbonic Anhydrase IX in Mice with Hypoxic HT29 Colorectal Tumor Xenografts. *PLoS ONE,* **2010**, *5*, 1-9.

18. Pastorek, J.; Pastorekova, S. Hypoxia-induced carbonic anhydrase IX as a target for cancer therapy: From biology to clinical use. *Semin. Cancer Biol.* **2015**, *31*, 52-64.

19. Swietach, P.; Vaughan-Jones, R. D.; Harris, A. L. Regulation of tumor pH and the role of carbonic anhydrase 9. *Cancer Metastasis Rev.* **2007**, *26*, 299-310.

20. Parks, S. K.; Chiche, J.; Pouyssegur, J. pH control mechanisms of tumor survival and growth. *J. Cell. Physiol.* **2011**, *226*, 299-308.

21. Oosterwdk, E.; Ruiter, D. J.; Hoedemaeker, P. J.; Pauwels, E. K. J.; Jonas, U.; Zwartendijk, I.; Warnaar, S. O. Monoclonal antibody G 250 recognizes a determinant present in renal-cell carcinoma and absent from normal kidney. *Int. J. Cancer,* **1986**, *38*, 489-494.

22. Sneddon, D.; Poulsen, S.-A. Agents described in the Molecular Imaging and Contrast Agent Database for imaging carbonic anhydrase IX expression. *J. Enzym. Inhib. Med. Chem.* **2014**, 29, 753-763.

23. Dubois, L. J.; Niemans, R.; van Kuijk, S. J. A.; Panth, K. M.; Parvathaneni, N.-K.; Peeters, S. G. J. A.; Zegers, C. M. L.; Rekers, N. H.; van Gisbergen, M. W.; Biemans, R.; Lieuwes, N. G.; Spiegelberg, L.; Yaromina, A.; Winum, J.-Y.; Vooijs, M.; Lambin, P. New ways to image and target tumour hypoxia and its molecular responses. *Radiother. Oncol.* **2015**, *116*, 352-357.

24. Dubois, L.; Douma, K.; Supuran, C. T.; Chiu, R. K.; van Zandvoort, M. A. M. J.; Pastoreková, S.; Scozzafava, A.; Wouters, B. G.; Lambin, P. Imaging the hypoxia surrogate marker CA IX requires expression and catalytic activity for binding fluorescent sulfonamide inhibitors. *Radiother. Oncol.* **2007**, *83*, 367-373.

25. Doss, M.; Kolb, H. C.; Walsh, J. C.; Mocharla, V. P.; Zhu, Z.; Haka, M.; Alpaugh, R. K.; Chen, D. Y. T.; Yu, J. Q. Biodistribution and Radiation Dosimetry of the Carbonic Anhydrase IX Imaging Agent [18 F]VM4-037 Determined from PET/CT Scans in Healthy Volunteers. *Mol. Imaging Biol.* **2014**, *16*, 739-746.

26. Lau, J.; Liu, Z.; Lin, K.-S.; Pan, J.; Zhang, Z.; Vullo, D.; Supuran, C. T.; Perrin, D. M.; Bénard, F. Trimeric Radiofluorinated Sulfonamide Derivatives to Achieve In Vivo Selectivity for Carbonic Anhydrase IX–Targeted PET Imaging. *J. Nucl. Med.* **2015**, *56*, 1434-1440.

27. Lau, J.; Zhang, Z.; Jenni, S.; Kuo, H.-T.; Liu, Z.; Vullo, D.; Supuran, C. T.; Lin, K.-S.; Bénard, F. PET imaging of carbonic anhydrase IX expression of HT-29 tumor xenograft mice with 68Ga-labeled benzenesulfonamides. *Mol. Pharm.* **2016**, *13*, 1137-1146

28. Pan, J.; Lau, J.; Mesak, F.; Hundal, N.; Pourghiasian, M.; Liu, Z.; Bénard, F.; Dedhar, S.; Supuran, C. T.; Lin, K.-S. Synthesis and evaluation of 18F-labeled carbonic anhydrase IX inhibitors for imaging with positron emission tomography. *J. Enzym. Inhib. Med. Chem.* **2014**, *29*, 249-255.

29. Day, J. A.; Cohen, S. M. Investigating the Selectivity of Metalloenzyme Inhibitors. *J. Med. Chem.* **2013**, *56*, 7997-8007.

30. Peeters, S. J. A.; Dubois, L.; Lieuwes, N.; Laan, D.; Mooijer, M.; Schuit, R.; Vullo, D.; Supuran, C.; Eriksson, J.; Windhorst, A.; Lambin, P. [18F]VM4-037 MicroPET Imaging and Biodistribution of Two In Vivo CAIX-Expressing Tumor Models. *Mol. Imaging Biol.* **2015**, *17*, 615-619.

31. Metwalli, A. R.; Turkbey, B.; McKinney, Y.; Weaver, J.; Yaqub-Ogun, N.; Merino, M.; Lindenberg, M. L.; Linehan, W. M.; Choyke, P. L. Results of a phase II trial of novel carbonic anhydrase IX radiotracer 18F-VM4-037 in renal cell carcinoma. In *2014 Genitourinary Cancer Symposium*, San Francisco, USA, 2014.

32. Turkbey, B.; Lindenberg, M. L.; Adler, S.; Kurdziel, K. A.; McKinney, Y. L.; Weaver, J.; Vocke, C. D.; Anver, M.; Bratslavsky, G.; Eclarinal, P.; Kwarteng, G.; Lin, F. I.; Yaqub-Ogun, N.; Merino, M. J.; Marston Linehan, W.; Choyke, P. L.; Metwalli, A. R. PET/CT imaging of renal cell carcinoma with 18F-VM4-037: a phase II pilot study. *Abdom. Radiol.* **2015**, *41*, 109-118.

33. Velikyan, I. Prospective of (68)Ga-Radiopharmaceutical Development. *Theranostics* **2014**, 4, 47-80.

34. Ambrosini, V.; Tomassetti, P.; Franci, R.; Fanti, S. Imaging of NETs with PET radiopharmaceuticals. *Q. J. Nucl. Med. Mol. Imaging* **2010**, *54*, 16-23.

35. Carter, N. D.; Heath, R.; Welty, R. J.; Hewe'It-Emmett, D.; Jeffery, S.; Shiels, A.; Tashian, R. E. Red Cells Genetically Deficient in Carbonic Anhydrase II Have Elevated Levels of a Carbonic Anhydrase Indistinguishable from Muscle CA IIIa. *Ann. N.Y. Acad. Sci.* **1984**, *429*, 284-286.

36. Akurathi, V.; Dubois, L.; Celen, S.; Lieuwes, N. G.; Chitneni, S. K.; Cleynhens, B. J.; Innocenti, A.; Supuran, C. T.; Verbruggen, A. M.; Lambin, P.; Bormans, G. M. Development and biological evaluation of 99mTc-sulfonamide derivatives for in vivo visualization of CA IX as surrogate tumor hypoxia markers. *Eur. J. Med. Chem.* **2014**, *71*, 374-384.

37. Akurathi, V.; Dubois, L.; Lieuwes, N. G.; Chitneni, S. K.; Cleynhens, B. J.; Vullo, D.; Supuran, C. T.; Verbruggen, A. M.; Lambin, P.; Bormans, G. M. Synthesis and biological evaluation of a 99mTc-labelled sulfonamide conjugate for in vivo visualization of carbonic anhydrase IX expression in tumor hypoxia. *Nuc. Med. Biol.* **2010**, *37*, 557-564.

38. Lopez, M.; Salmon, A. J.; Supuran, C. T.; Poulsen, S.-A. Carbonic Anhydrase Inhibitors Developed Through "Click Tailing". *Curr. Pharm. Des.* **2010**, *16*, 3277-3287.

39. Lopez, M.; Drillaud, N.; Bornaghi, L. F.; Poulsen, S.-A. Synthesis of S-Glycosyl Primary Sulfonamides. *J. Org. Chem.* **2009**, *74*, 2811-2816.

40. Salmon, A. J.; Williams, M. L.; Maresca, A.; Supuran, C. T.; Poulsen, S.-A. Synthesis of glycoconjugate carbonic anhydrase inhibitors by ruthenium-catalysed azide-alkyne 1,3-dipolar cycloaddition. *Bioorg. Med. Chem. Lett.* **2011**, *21*, 6058-6061.

41. Rankin, G. M.; Vullo, D.; Supuran, C. T.; Poulsen, S.-A. Phosphate Chemical Probes Designed for Location Specific Inhibition of Intracellular Carbonic Anhydrases. *J. Med. Chem.* **2015**, 58, 7580-7590.

42. Moeker, J.; Mahon, B. P.; Bornaghi, L. F.; Vullo, D.; Supuran, C. T.; McKenna, R.; Poulsen, S.-A. Structural Insights into Carbonic Anhydrase IX Isoform Specificity of Carbohydrate-Based Sulfamates. *J. Med. Chem.* **2014**, *57*, 8635-8645.

43. Poulsen, S.-A. Carbonic anhydrase inhibition as a cancer therapy: a review of patent literature, 2007 – 2009. *Expert Opin. Ther. Pat.* **2010**, *20*, 795-806.

44. Price, E. W.; Orvig, C. Matching chelators to radiometals for radiopharmaceuticals. *Chem. Soc. Rev.* **2014**, *43*, 260-290.

45. Mojtahedi, A.; Thamake, S.; Tworowska, I.; Ranganathan, D.; Delpassand, E. S. The value of (68)Ga-DOTATATE PET/CT in diagnosis and management of neuroendocrine tumors compared to current FDA approved imaging modalities: a review of literature. *Am. J. Nucl. Med. Mol. Imaging* **2014**, *4*, 426-434.

46. Eder, M.; Neels, O.; Müller, M.; Bauder-Wüst, U.; Remde, Y.; Schäfer, M.; Hennrich, U.; Eisenhut, M.; Afshar-Oromieh, A.; Haberkorn, U.; Kopka, K. Novel Preclinical and Radiopharmaceutical Aspects of [(68)Ga]Ga-PSMA-HBED-CC: A New PET Tracer for Imaging of Prostate Cancer. *Pharmaceuticals* **2014**, *7*, 779-796.

47. Meldal, M.; Tornøe, C. W. Cu-Catalyzed Azide−Alkyne Cycloaddition. *Chem. Rev.* **2008**, *108*, 2952-3015.

48. Tron, G. C.; Pirali, T.; Billington, R. A.; Canonico, P. L.; Sorba, G.; Genazzani, A. A. Click chemistry reactions in medicinal chemistry: Applications of the 1,3-dipolar cycloaddition between azides and alkynes. *Med. Res. Rev.* **2008**, *28*, 278-308.

49. Kadajji, V. G.; Betageri, G. V. Water Soluble Polymers for Pharmaceutical Applications. *Polymers* **2011**, *3*, 1972-2009.

50. Knop, K.; Hoogenboom, R.; Fischer, D.; Schubert, U. S. Poly(ethylene glycol) in Drug Delivery: Pros and Cons as Well as Potential Alternatives. *Angew. Chem. Int. Ed.* **2010**, *49*, 6288-6308.

51. Rami, M.; Cecchi, A.; Montero, J.-L.; Innocenti, A.; Vullo, D.; Scozzafava, A.; Winum, J.-Y.; Supuran, C. T. Carbonic Anhydrase Inhibitors: Design of Membrane-Impermeant Copper(II) Complexes of DTPA-, DOTA-, and TETA-Tailed Sulfonamides Targeting the Tumor-Associated Transmembrane Isoform IX. *ChemMedChem* **2008**, *3*, 1780-1788.

52. Rami, M.; Montero, J.-L.; Dubois, L.; Lambin, P.; Scozzafava, A.; Winum, J.-Y.; Supuran, C. T. Carbonic anhydrase inhibitors: Gd(iii) complexes of DOTA- and TETA-sulfonamide conjugates

targeting the tumor associated carbonic anhydrase isozymes IX and XII. *New J. Chem.* **2010**, *34*, 2139-2144.

53. Wilkinson, B. L.; Innocenti, A.; Vullo, D.; Supuran, C. T.; Poulsen, S.-A. Inhibition of Carbonic Anhydrases with Glycosyltriazole Benzene Sulfonamides. *J. Med. Chem.* **2008**, *51*, 1945-1953.

54. Hannant, J.; Hedley, J. H.; Pate, J.; Walli, A.; Farha Al-Said, S. A.; Galindo, M. A.; Connolly, B. A.; Horrocks, B. R.; Houlton, A.; Pike, A. R. Modification of DNA-templated conductive polymer nanowires via click chemistry. *Chem. Commun.* **2010**, *46*, 5870-5872.

55. Barnett, D. J. Radiopharmaceutical compositions. In Google Patents: 2012.

56. Prasuhn, J. D. E.; Yeh, R. M.; Obenaus, A.; Manchester, M.; Finn, M. G. Viral MRI contrast agents: coordination of Gd by native virions and attachment of Gd complexes by azide-alkyne cycloaddition. *Chem. Commun.* **2007**, 1269-1271.

57. Supuran, C. T.; Scozzafava, A. Benzolamide is not a Membrane-impermeant Carbonic Anhydrase Inhibitor. *J. Enzym. Inhib. Med. Chem.* **2004**, *19*, 269-273.

58. Khalifah, R. G. The Carbon Dioxide Hydration Activity of Carbonic Anhydrase: I. Stop-flow Kinetic Studies on the Native Human Isoenzymes B and C. *J. Biol. Chem.* **1971**, *246*, 2561-2573.

59. Rami, M.; Dubois, L.; Parvathaneni, N.-K.; Alterio, V.; van Kuijk, S. J. A.; Monti, S. M.; Lambin, P.; De Simone, G.; Supuran, C. T.; Winum, J.-Y. Hypoxia-Targeting Carbonic Anhydrase IX Inhibitors by a New Series of Nitroimidazole-Sulfonamides/Sulfamides/Sulfamates. *J. Med. Chem.* **2013**, *56*, 8512-8520.

60. Dubois, L.; Peeters, S. G. J. A.; van Kuijk, S. J. A.; Yaromina, A.; Lieuwes, N. G.; Saraya, R.; Biemans, R.; Rami, M.; Parvathaneni, N. K.; Vullo, D.; Vooijs, M.; Supuran, C. T.; Winum, J.-Y.; Lambin, P. Targeting carbonic anhydrase IX by nitroimidazole based sulfamides enhances the therapeutic effect of tumor irradiation: A new concept of dual targeting drugs. *Radiother. Oncol.* **2013**, *108*, 523-528.

61. Dubois, L.; Peeters, S.; Lieuwes, N. G.; Geusens, N.; Thiry, A.; Wigfield, S.; Carta, F.; McIntyre, A.; Scozzafava, A.; Dogné, J.-M.; Supuran, C. T.; Harris, A. L.; Masereel, B.; Lambin, P.

Specific inhibition of carbonic anhydrase IX activity enhances the in vivo therapeutic effect of tumor irradiation. *Radiother. Oncol.* **2011**, *99*, 424-431.

62. Lam, C. F. C.; Giddens, A. C.; Chand, N.; Webb, V. L.; Copp, B. R. Semi-synthesis of bioactive fluorescent analogues of the cytotoxic marine alkaloid discorhabdin C. *Tetrahedron* **2012**, *68*, 3187-3194.

63. Bakleh, M. E.; Sol, V.; Estieu-Gionnet, K.; Granet, R.; Déléris, G.; Krausz, P. An efficient route to VEGF-like peptide porphyrin conjugates via microwave-assisted 'click-chemistry'. *Tetrahedron* **2009**, *65*, 7385-7392.

64. Goswami, L. N.; Houston, Z. H.; Sarma, S. J.; Jalisatgi, S. S.; Hawthorne, M. F. Efficient synthesis of diverse heterobifunctionalized clickable oligo(ethylene glycol) linkers: potential applications in bioconjugation and targeted drug delivery. *Org. Biomol. Chem.* **2013**, *11*, 1116-1126.

65. Raghunand, N.; Guntle, G. P.; Gokhale, V.; Nichol, G. S.; Mash, E. A.; Jagadish, B. Design, Synthesis, and Evaluation of 1,4,7,10-Tetraazacyclododecane-1,4,7-triacetic Acid Derived, Redox-Sensitive Contrast Agents for Magnetic Resonance Imaging. *J. Med. Chem.* **2010**, *53*, 6747-6757.

66. Kale, R. R.; Clancy, C. M.; Vermillion, R. M.; Johnson, E. A.; Iyer, S. S. Synthesis of soluble multivalent glycoconjugates that target the Hc region of botulinum neurotoxin A. *Bioorg. Med. Chem. Lett.* **2007**, *17*, 2459-2464.

67. Ščasnár, V.; Lier, J. E. The use of SEP-PAK Sl cartridges for the preparation of gallium chloride from the citrate solution. *Eur. J. Nucl. Med. 20*, 273-273.

68. Winum, J.-Y.; Vullo, D.; Casini, A.; Montero, J.-L.; Scozzafava, A.; Supuran, C. T. Carbonic Anhydrase Inhibitors. Inhibition of Cytosolic Isozymes I and II and Transmembrane, Tumor-Associated Isozyme IX with Sulfamates Including EMATE Also Acting as Steroid Sulfatase Inhibitors. *J. Med. Chem.* **2003**, *46*, 2197-2204.

69. Vullo, D.; Innocenti, A.; Nishimori, I.; Pastorek, J. r.; Scozzafava, A.; Pastoreková, S.; Supuran, C. T. Carbonic anhydrase inhibitors. Inhibition of the transmembrane isozyme XII with sulfonamides—a new target for the design of antitumor and antiglaucoma drugs? *Bioorg. Med. Chem. Lett.* **2005**, *15*, 963-969.

Table of Contents graphic